Monthly Notices
of the
ROYAL ASTRONOMICAL SOCIETY

MNRAS **447,** 3342–3360 (2015) doi:10.1093/mnras/stu2678

On the variation of Fourier parameters for Galactic and LMC Cepheids at optical, near-infrared and mid-infrared wavelengths

Anupam Bhardwaj,[1⋆] Shashi M. Kanbur,[2] Harinder P. Singh,[1] Lucas M. Macri[3] and Chow-Choong Ngeow[4]

[1]*Department of Physics & Astrophysics, University of Delhi, Delhi 110007, India*
[2]*State University of New York, Oswego, NY 13126, USA*
[3]*Mitchell Institute for Fundamental Physics & Astronomy, Department of Physics & Astronomy, Texas A&M University, College Station, TX 77843, USA*
[4]*Graduate Institute of Astronomy, National Central University, Jhongli 32001, Taiwan*

Accepted 2014 December 15. Received 2014 December 15; in original form 2014 July 29

ABSTRACT

We present a light-curve analysis of fundamental-mode Galactic and Large Magellanic Cloud (LMC) Cepheids based on the Fourier decomposition technique. We have compiled light-curve data for Galactic and LMC Cepheids in optical (*VI*), near-infrared (JHK_s) and mid-infrared (3.6 and 4.5 μm) bands from the literature and determined the variation of their Fourier parameters as a function of period and wavelength. We observed a decrease in Fourier amplitude parameters and an increase in Fourier phase parameters with increasing wavelengths at a given period. We also found a decrease in the skewness and acuteness parameters as a function of wavelength at a fixed period. We applied a binning method to analyse the progression of the mean Fourier parameters with period and wavelength. We found that for periods longer than about 20 d, the values of the Fourier amplitude parameters increase sharply for shorter wavelengths as compared to wavelengths longer than the *J* band. We observed the variation of the Hertzsprung progression with wavelength. The central period of the Hertzsprung progression was found to increase with wavelength in the case of the Fourier amplitude parameters and decrease with increasing wavelength in the case of phase parameters. We also observed a small variation of the central period of the progression between the Galaxy and LMC, presumably related to metallicity effects. These results will provide useful constraints for stellar pulsation codes that incorporate stellar atmosphere models to produce Cepheid light curves in various bands.

Key words: stars: variables: Cepheids – Magellanic Clouds.

1 INTRODUCTION

Cepheid variables are bright, Population I periodic radial pulsators that exhibit regular light curves and obey a well-known period–luminosity relation (Leavitt & Pickering 1912), that is an important tool in the extragalactic distance scale. Fourier analysis methods have been used extensively to describe Cepheid light-curve structure and its variation with period. In particular, the amplitude ratios (R_{21} and R_{31}) and phase differences (ϕ_{21} and ϕ_{31}) have been used to quantitatively describe the progression of Cepheid light-curve shape with period (Simon 1977). The Fourier decomposition method was further revived by Simon & Lee (1981), who used a sample of 57 Cepheids and discussed the variation of Fourier parameters with period. The sharp breaks in the progressions of Fourier parameters with period, occurring near 10 d, were attributed to the resonance $P_2/P_0 = 0.5$, in the normal mode spectrum (Simon & Schmidt 1976; Simon 1977; Simon & Lee 1981). Later, the method was used extensively by Simon & Teays (1982) to analyse the progressions of Fourier parameters and light-curve structure of a large sample of field RR Lyrae stars. The light and velocity curves were Fourier decomposed to compare with theoretically modelled light curves (Simon & Davis 1983; Simon & Moffett 1985). Similar studies of the light-curve structures of RR Lyrae variables were carried out by Simon (1985) and Kovacs, Shlosman & Buchler (1986). The Fourier phase parameter (ϕ_{31}) was used in empirical relations to determine the metallicity of fundamental mode RR Lyrae stars (Jurcsik & Kovacs 1996). The studies on theoretical light curves of Cepheid variables using the skewness and acuteness parameters together with the variation of Fourier parameters were carried out by Stellingwerf & Donohoe (1986, 1987) and Bono, Marconi & Stellingwerf (2000). The central period of Hertzsprung progression was also determined using the Fourier parameters (Moskalik, Buchler & Marom 1992; Welch et al. 1997; Beaulieu

⋆ E-mail: anupam.bhardwajj@gmail.com

1998) and skewness/acuteness parameters (Bono et al. 2000). Other studies employing the Fourier decomposition technique to analyse the light curves of Cepheid variables are Simon (1986, 1988), Antonello & Poretti (1986), Andreasen & Petersen (1987), Andreasen (1988), Poretti (1994), Simon & Kanbur (1995), Stetson (1996), Welch et al. (1997) and Beaulieu (1998).

Recent applications of this method include the reconstruction of Cepheid light curves with Fourier technique (Ngeow et al. 2003), and classification of variable star light curves based on Fourier parameters and Principal Component Analysis (Deb & Singh 2009). Most of the recent studies on Fourier decomposition involve the determination of physical parameters like absolute magnitude, metallicity, effective temperature, luminosity for RR Lyrae variables (Deb & Singh 2010; Nemec et al. 2011). The Fourier decomposition technique has been further extended to describe the chemical and structural properties of the LMC (Deb & Singh 2014).

In this work, we analyse the light curves of fundamental-mode Galactic and LMC Cepheids in multiple bands using Fourier decomposition techniques. In Section 2, we provide a brief description of the application of the Fourier decomposition method. In Section 3, we discuss the Galactic and LMC Cepheid light-curve data compiled from the literature for optical, near-infrared and mid-infrared wavelengths. In Section 4, we describe the application of Fourier decomposition to Galactic and LMC Cepheid light curves. Further, we discuss the variation of Fourier parameters with period in each band separately. In Section 5, we compare the Fourier parameters in multiple bands and comment on their progression with period and wavelength. We also discuss the variation of mean Fourier parameters together with skewness and acuteness parameters as a function of wavelength at a given period. In Section 6, we summarize the variation of the central period of the Hertzsprung progression with wavelength for each Fourier parameter in the Galaxy and LMC. A discussion on our results and important conclusions arising from this study are presented in Section 7.

Our results will provide important constraints for stellar pulsation codes that incorporate stellar atmosphere models to produce wavelength-dependent theoretical Cepheid light curves.

2 FOURIER DECOMPOSITION TECHNIQUE

Fourier decomposition is a robust method to study the light curves of variable stars. This method was revived and refined by Simon & Lee (1981) in its modern form. They described how the lower order Fourier coefficients can completely describe the structure of the light curve. The Fourier coefficients and Fourier parameters are now widely used to derive empirical relations to determine physical parameters of variable stars, in particular for fundamental mode RR Lyrae stars.

In this study, we have used a sine Fourier series to fit the multiband light curves of Galactic and LMC Cepheids,

$$m(t) = m_0 + \sum_{i=1}^{N} A_i \sin(i\omega(t - t_0) + \phi_i), \quad (1)$$

where $m(t)$ is the observed magnitude, m_0 is the mean magnitude from the Fourier fit, t is the time of observation, $\omega = 2\pi/P$ is the angular frequency and t_0 corresponds to the epoch of maximum brightness. In this study, we have taken t_0 as the time of minimum magnitude from the light-curve data for each Cepheid, which is used to obtain a phased light curve that has maximum light at phase zero. A_i and ϕ_i are amplitude and phase coefficients, respectively. Since the period P is known, the light curves are phased using

$$x = \mathrm{frac}\left(\frac{t - t_0}{P}\right).$$

Since the values of x range from 0 to 1, corresponding to a full cycle of pulsation, equation (1) can be written as

$$m = m_0 + \sum_{i=1}^{N} A_i \sin(2\pi i x + \phi_i). \quad (2)$$

Here, N is the optimum order of fit, which is generally chosen depending on the size of least square residuals. Furthermore, coefficients $A_1, \ldots, A_N$ and $\phi_1, \ldots, \phi_N$ are extracted from the fit to give Fourier parameters,

$$R_{i1} = \frac{A_i}{A_1}; \phi_{i1} = \phi_i - i\phi_1, \quad (3)$$

where $i > 1$. The ϕ_{i1} are generally adjusted to lie between 0 and 2π. The errors in the derived Fourier parameters are determined using the propagation of errors in the coefficients (Deb & Singh 2010).

3 THE DATA

The data selected for present analysis are described in Table 1. A brief description of each catalogue/source used is presented in the following subsections.

Table 1. The Galactic and LMC Cepheid multiwavelength light-curve data selected for the present analysis.

Band	Galaxy		LMC	
	No. of stars	References	No. of stars	References
V	447	Berdnikov (1995)	1832	Soszynski et al. (2008); Ulaczyk et al. (2013)
I	351	–	1844	–
J	186	Welch et al. (1984); Laney & Stobie (1992); Barnes et al. (1997); Monson & Pierce (2011)	474	Macri et al. (2014); Persson et al. (2004)
H	186	–	532	–
K_s	186	–	488	–
3.6 μm	37	Monson et al. (2012)	84	Scowcroft et al. (2011)
4.5 μm	37	–	84	–

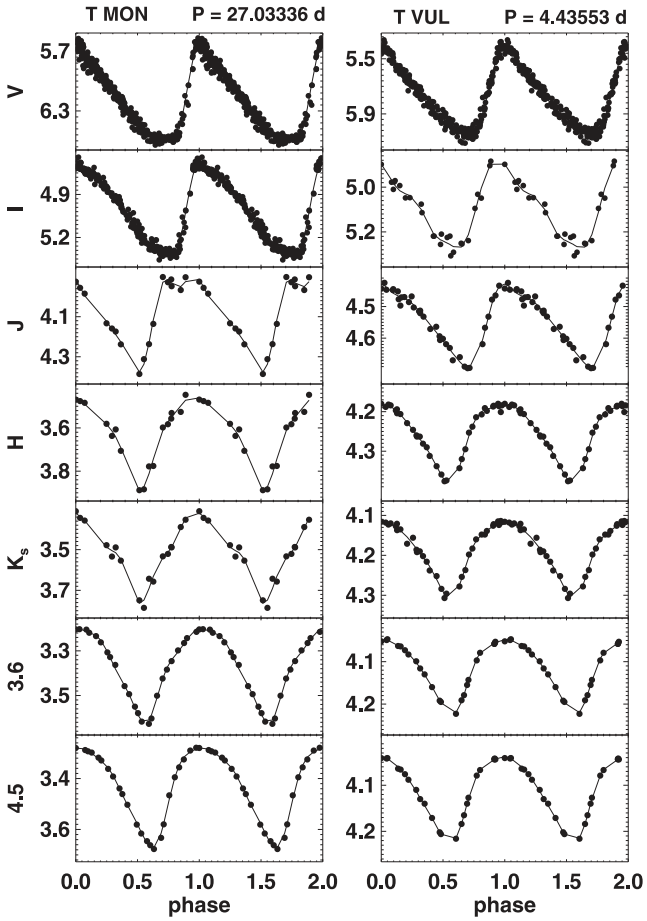

Figure 1. Examples of the Fourier-fitted light curves of two Galactic Cepheids in multiple bands. The star ID is given at the top of each panel.

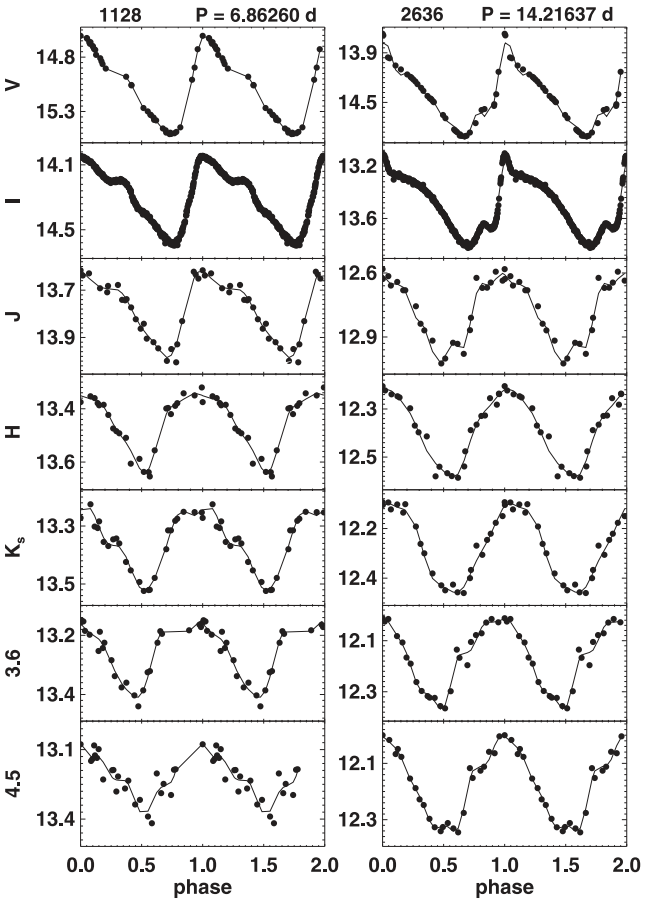

Figure 2. Same as Fig. 1, but for two LMC Cepheids. Star ID's consisting of four numbers are based on the OGLE-III catalogue. These variables are identified as HV2337 and HV1006 in Persson et al. (2004) and Scowcroft et al. (2011).

3.1 Optical wavelengths

3.1.1 Galactic Cepheids

The light-curve data for Galactic Cepheids in the Johnson *V* and Kron–Cousins *I* bands were extracted from the catalogue of Berdnikov (1995). This catalogue gathers photoelectric observations of Galactic Cepheids made between 1986 and 2004 by Berdnikov and his collaborators in a series of papers (Berdnikov 1987, 1992; Berdnikov & Yakubov 1993; Berdnikov & Vozyakova 1995; Berdnikov, Ignatova & Pastukhova 1998; Berdnikov & Turner 2001, 2004a,b). Our analysis makes use of 447 and 351 Galactic Cepheids with data in the *V* and *I* bands, respectively. Since this catalogue is compiled from a series of observations carried out over two decades, the number of data points for each star ranges from 20 to nearly 400. The periods of the variables were extracted from the data base of Galactic Classical Cepheids (Fernie et al. 1995).

3.1.2 LMC Cepheids

The light-curve data for LMC Cepheids in the *V* and *I* bands were taken from the third phase of the Optical Gravitational Lensing Experiment (OGLE-III) survey (Soszynski et al. 2008). The observations were carried out using a dedicated 1.3-m telescope at the Las Campanas Observatory, Chile. Our analysis makes use of 1806 and 1818 light curves in the *V* and *I* bands, respectively. The light curves are fairly well sampled with a large number of data points in *I* band, and covering nearly full phase in both optical bands. We also make use of the period and initial epoch provided in this data base to Fourier fit the light curves.

We also extracted the light-curve data in the *V* and *I* bands for 26 long-period Cepheids from OGLE-III Shallow Survey in the LMC (Ulaczyk et al. 2013). The photometric data for these Cepheids were also collected using the 1.3-m Warsaw Telescope located at Las Campanas Observatory. Since the photometric system is exactly similar in both the surveys (Soszynski et al. 2008; Ulaczyk et al. 2013), we increase our sample to have 1832 Cepheids in *V* band and 1844 Cepheids in *I* band.

3.2 Near-infrared wavelengths

3.2.1 Galactic Cepheids

We compiled photometric data for 186 Galactic Cepheids in the JHK_s bands with full phase coverage using several sources in the literature (Welch et al. 1984; Laney & Stobie 1992; Barnes et al. 1997; Monson & Pierce 2011). The light curves taken from Monson & Pierce (2011) for 129 Galactic Cepheids were obtained during a span of 10 months in 2008 using the BIRCAM instrument at the 0.6-m telescope of the University of Wyoming Red Buttes Observatory. These light curves have an average of 22 observations per star, providing reasonable phase coverage. We included 41 light curves

Table 2. Fourier parameters obtained using a sine series Fourier fit to the Galactic Cepheid light curves in multibands.

Star ID	log (*P*)	t_0 (JD)	*N*	$S_k(V)$	$A_c(V)$	$A_1(V)$	$\phi_1(V)$	$R_{21}(V)$	$R_{31}(V)$	$\phi_{21}(V)$	$\phi_{31}(V)$
						$\sigma_{A_1(V)}$	$\sigma_{\phi_1(V)}$	$\sigma_{R_{21}(V)}$	$\sigma_{R_{31}(V)}$	$\sigma_{\phi_{21}(V)}$	$\sigma_{\phi_{31}(V)}$
AA GEM	1.053 17	245 0327.50	4	1.150 54	1.293 58	0.284 74	4.546 09	0.045 94	0.148 52	1.159 55	3.449 48
						0.000 18	0.000 62	0.000 63	0.000 64	0.013 19	0.004 63
AA MON	0.595 29	244 9805.60	4	3.444 44	1.518 89	0.280 38	4.047 57	0.394 47	0.223 37	2.563 12	5.536 55
						0.000 91	0.002 59	0.001 58	0.003 26	0.011 15	0.015 08
Star ID	log (*P*)	t_0 (JD)	*N*	$S_k(I)$	$A_c(I)$	$A_1(I)$	$\phi_1(I)$	$R_{21}(I)$	$R_{31}(I)$	$\phi_{21}(I)$	$\phi_{31}(I)$
						$\sigma_{A_1(I)}$	$\sigma_{\phi_1(I)}$	$\sigma_{R_{21}(I)}$	$\sigma_{R_{31}(I)}$	$\sigma_{\phi_{21}(I)}$	$\sigma_{\phi_{31}(I)}$
AA MON	0.595 29	244 9809.60	4	1.985 07	1.375 30	0.166 41	3.926 83	0.424 73	0.253 41	3.188 26	6.216 61
						0.000 92	0.004 27	0.003 11	0.005 59	0.017 36	0.023 06
AA SER	1.234 04	245 1255.60	4	1.469 14	1.298 85	0.253 41	4.370 60	0.204 65	0.123 24	2.912 94	5.098 47
						0.000 15	0.000 62	0.000 64	0.000 60	0.003 13	0.005 38
Star ID	log (*P*)	t_0 (JD)	*N*	$S_k(J)$	$A_c(J)$	$A_1(J)$	$\phi_1(J)$	$R_{21}(J)$	$R_{31}(J)$	$\phi_{21}(J)$	$\phi_{31}(J)$
						$\sigma_{A_1(J)}$	$\sigma_{\phi_1(J)}$	$\sigma_{R_{21}(J)}$	$\sigma_{R_{31}(J)}$	$\sigma_{\phi_{21}(J)}$	$\sigma_{\phi_{31}(J)}$
AA GEM	1.053 20	245 4487.90	4	1.304 15	0.930 50	0.093 33	4.353 33	0.117 86	0.111 75	3.080 27	5.073 97
						0.004 20	0.044 00	0.044 89	0.045 71	0.391 12	0.417 52
AA MON	0.595 30	245 4523.80	5	1.732 24	0.620 75	0.137 59	3.976 21	0.307 73	0.099 35	3.680 45	0.612 30
						0.010 07	0.071 83	0.043 12	0.062 71	0.282 93	0.617 63
Star ID	log (*P*)	t_0 (JD)	*N*	$S_k(H)$	$A_c(H)$	$A_1(H)$	$\phi_1(H)$	$R_{21}(H)$	$R_{31}(H)$	$\phi_{21}(H)$	$\phi_{31}(H)$
						$\sigma_{A_1(H)}$	$\sigma_{\phi_1(H)}$	$\sigma_{R_{21}(H)}$	$\sigma_{R_{31}(H)}$	$\sigma_{\phi_{21}(H)}$	$\sigma_{\phi_{31}(H)}$
AA GEM	1.053 20	245 4579.70	4	1.288 33	0.818 18	0.103 83	4.438 51	0.113 84	0.028 41	4.079 90	4.470 53
						0.003 85	0.037 27	0.037 41	0.038 54	0.337 27	1.283 16
AA MON	0.595 30	245 4516.80	4	0.754 39	0.324 50	0.101 27	5.124 93	0.341 07	0.252 89	4.430 58	2.005 80
						0.006 82	0.066 74	0.052 94	0.063 07	0.250 83	0.339 18
Star ID	log (*P*)	t_0 (JD)	*N*	$S_k(K_s)$	$A_c(K_s)$	$A_1(K_s)$	$\phi_1(K_s)$	$R_{21}(K_s)$	$R_{31}(K_s)$	$\phi_{21}(K_s)$	$\phi_{31}(K_s)$
						$\sigma_{A_1(K_s)}$	$\sigma_{\phi_1(K_s)}$	$\sigma_{R_{21}(K_s)}$	$\sigma_{R_{31}(K_s)}$	$\sigma_{\phi_{21}(K_s)}$	$\sigma_{\phi_{31}(K_s)}$
AA GEM	1.053 20	245 4579.70	4	0.795 33	0.727 12	0.114 88	0.128 56	0.127 18	0.037 95	5.011 38	3.954 53
						0.005 93	0.051 71	0.05281	0.054 53	0.417 51	1.312 82
AA MON	0.595 30	245 4492.80	5	1.551 02	0.353 18	0.093 32	5.169 33	0.39145	0.241 75	4.524 06	2.114 36
						0.010 86	0.144 67	0.081 71	0.117 54	0.450 03	0.606 24
Star ID	log (*P*)	t_0 (JD)	*N*	$S_k(3.6)$	$A_c(3.6)$	$A_1(3.6)$	$\phi_1(3.6)$	$R_{21}(3.6)$	$R_{31}(3.6)$	$\phi_{21}(3.6)$	$\phi_{31}(3.6)$
						$\sigma_{A_1(3.6)}$	$\sigma_{\phi_1(3.6)}$	$\sigma_{R_{21}(3.6)}$	$\sigma_{R_{31}(3.6)}$	$\sigma_{\phi_{21}(3.6)}$	$\sigma_{\phi_{31}(3.6)}$
BETA DOR	0.993 00	245 5185.614	4	0.661 13	0.919 39	0.094 93	4.817 00	0.127 78	0.025 70	5.973 77	0.572 82
						0.005 16	0.044 90	0.052 71	0.051 11	0.419 66	1.979 51
CD CYG	1.232 00	245 5370.893	4	1.257 34	0.631 32	0.181 64	4.865 87	0.170 23	0.064 85	4.514 43	2.562 12
						0.003 68	0.015 84	0.019 20	0.018 76	0.107 26	0.261 34
Star ID	log (*P*)	t_0 (JD)	*N*	$S_k(4.5)$	$A_c(4.5)$	$A_1(4.5)$	$\phi_1(4.5)$	$R_{21}(4.5)$	$R_{31}(4.5)$	$\phi_{21}(4.5)$	$\phi_{31}(4.5)$
						$\sigma_{A_1(4.5)}$	$\sigma_{\phi_1(4.5)}$	$\sigma_{R_{21}(4.5)}$	$\sigma_{R_{31}(4.5)}$	$\sigma_{\phi_{21}(4.5)}$	$\sigma_{\phi_{31}(4.5)}$
BETA DOR	0.993 00	245 5176.550	4	0.666 67	0.980 20	0.096 32	5.057 96	0.081 50	0.062 09	0.021 67	5.389 38
						0.002 96	0.028 14	0.027 21	0.026 54	0.403 79	0.528 05
CD CYG	1.232 00	245 5361.685	4	1.314 81	0.718 21	0.186 03	4.460 42	0.165 40	0.023 01	4.113 89	1.831 27
						0.001 60	0.009 24	0.008 93	0.010 38	0.060 42	0.356 69

Notes. This table is available entirely in a machine-readable form in the online journal as supporting information.

from Laney & Stobie (1992) that were obtained between 1982 and 1990 at the Sutherland observing station of South African Astronomical Observatory. Most of the observations were carried out using the 0.75-m telescope and the Mark II infrared photometer and the remaining observations were made using the 1.9-m telescope and the Mark III infrared photometer. These light curves have 31 data points per star. We also made use of eight light curves from Barnes et al. (1997) obtained at the 1.3-m telescope at Kitt Peak National Observatory using the OTTO and SQIID instruments. Lastly, we incorporated eight variables from Welch et al. (1984) that were obtained using the 1-m Swope telescope at Las Campanas Observation, Chile and the 0.6-m telescope at Mount Wilson using the 0.6-m reflector.

Since these near-infrared light-curve data were obtained by the various authors using different photometric systems, we transformed them into the 2MASS system using the transformations provided as part of their all-sky data release.[1]

3.2.2 *LMC Cepheids*

Our analysis made use of combined LMC near-infrared light-curve data for 474, 532 and 488 Cepheids in *J*, *H* and K_s, respectively, from the two sources listed below.

[1] http://www.ipac.caltech.edu/2mass/releases/allsky/doc/sec6_4b.html

Table 3. Fourier parameters obtained using a sine series Fourier fit to the LMC Cepheid light curves in multibands. The Star ID's are from corresponding catalogues listed in Table 1 for each band.

Star ID	log (*P*)	t_0 (JD)	*N*	$S_k(V)$	$A_c(V)$	$A_1(V)$	$\phi_1(V)$	$R_{21}(V)$	$R_{31}(V)$	$\phi_{21}(V)$	$\phi_{31}(V)$
						$\sigma_{A_1(V)}$	$\sigma_{\phi_1(V)}$	$\sigma_{R_{21}(V)}$	$\sigma_{R_{31}(V)}$	$\sigma_{\phi_{21}(V)}$	$\sigma_{\phi_{31}(V)}$
0002	0.493 89	245 2171.239	4	2.448 28	1.457 00	0.191 18	4.192 31	0.335 91	0.125 17	2.667 24	5.505 64
						0.001 75	0.008 44	0.009 51	0.008 60	0.030 24	0.077 21
0005	0.749 12	245 2171.781	4	2.952 57	1.331 00	0.345 00	3.974 19	0.452 17	0.166 09	3.036 06	5.914 11
						0.001 04	0.003 03	0.003 28	0.002 86	0.009 10	0.021 81
Star ID	log (*P*)	t_0 (JD)	*N*	$S_k(I)$	$A_c(I)$	$A_1(I)$	$\phi_1(I)$	$R_{21}(I)$	$R_{31}(I)$	$\phi_{21}(I)$	$\phi_{31}(I)$
						$\sigma_{A_1(I)}$	$\sigma_{\phi_1(I)}$	$\sigma_{R_{21}(I)}$	$\sigma_{R_{31}(I)}$	$\sigma_{\phi_{21}(I)}$	$\sigma_{\phi_{31}(I)}$
0002	0.493 89	245 2171.239	4	2.174 60	1.008 03	0.112 20	4.111 96	0.295 46	0.102 32	3.149 67	6.165 18
						0.000 51	0.004 70	0.004 74	0.004 57	0.018 56	0.048 14
0005	0.749 12	245 2171.781	8	3.149 38	0.773 05	0.208 66	3.849 36	0.431 13	0.166 73	3.401 30	0.253 59
						0.000 44	0.002 22	0.002 34	0.002 18	0.006 70	0.014 64
Star ID	log (*P*)	t_0 (JD)	*N*	$S_k(J)$	$A_c(J)$	$A_1(J)$	$\phi_1(J)$	$R_{21}(J)$	$R_{31}(J)$	$\phi_{21}(J)$	$\phi_{31}(J)$
						$\sigma_{A_1(J)}$	$\sigma_{\phi_1(J)}$	$\sigma_{R_{21}(J)}$	$\sigma_{R_{31}(J)}$	$\sigma_{\phi_{21}(J)}$	$\sigma_{\phi_{31}(J)}$
0504	1.158 12	245 4438.279	4	1.518 89	0.760 56	0.248 90	4.336 26	0.134 27	0.115 39	3.269 27	1.210 61
						0.016 04	0.073 10	0.103 46	0.092 34	0.247 31	0.532 70
0519	0.225 27	245 4422.182	6	0.926 78	0.683 50	0.225 71	3.814 31	0.281 87	0.163 13	3.917 09	1.589 20
						0.018 11	0.053 89	0.094 76	0.072 09	0.258 80	0.627 53
Star ID	log (*P*)	t_0 (JD)	*N*	$S_k(H)$	$A_c(H)$	$A_1(H)$	$\phi_1(H)$	$R_{21}(H)$	$R_{31}(H)$	$\phi_{21}(H)$	$\phi_{31}(H)$
						$\sigma_{A_1(H)}$	$\sigma_{\phi_1(H)}$	$\sigma_{R_{21}(H)}$	$\sigma_{R_{31}(H)}$	$\sigma_{\phi_{21}(H)}$	$\sigma_{\phi_{31}(H)}$
0494	0.435 68	245 4046.364	5	0.175 09	0.162 79	0.175 78	6.106 06	1.531 63	1.065 59	0.327 41	5.881 43
						0.065 25	0.518 83	0.804 57	0.595 04	1.039 15	1.562 41
0539	0.538 44	245 4426.226	4	0.776 20	1.192 98	0.215 35	3.325 30	0.348 78	0.356 07	6.180 24	2.343 90
						0.058 44	0.133 29	0.194 70	0.165 59	0.579 05	0.481 91
Star ID	log (*P*)	t_0 (JD)	*N*	$S_k(K_s)$	$A_c(K_s)$	$A_1(K_s)$	$\phi_1(K_s)$	$R_{21}(K_s)$	$R_{31}(K_s)$	$\phi_{21}(K_s)$	$\phi_{31}(K_s)$
						$\sigma_{A_1(K_s)}$	$\sigma_{\phi_1(K_s)}$	$\sigma_{R_{21}(K_s)}$	$\sigma_{R_{31}(K_s)}$	$\sigma_{\phi_{21}(K_s)}$	$\sigma_{\phi_{31}(K_s)}$
0499	0.946 01	245 4107.035	4	0.972 39	0.631 32	0.109 26	4.746 42	0.178 93	0.133 81	4.954 83	2.326 88
						0.012 08	0.153 20	0.138 89	0.137 72	1.024 75	1.135 11
0504	1.158 12	245 4426.228	6	0.675 04	3.347 83	0.141 47	4.556 04	0.298 16	0.435 43	5.490 06	3.309 83
						0.024 04	0.719 08	0.223 81	0.514 29	3.263 15	2.841 90
Star ID	log (*P*)	t_0 (JD)	*N*	$S_k(3.6)$	$A_c(3.6)$	$A_1(3.6)$	$\phi_1(3.6)$	$R_{21}(3.6)$	$R_{31}(3.6)$	$\phi_{21}(3.6)$	$\phi_{31}(3.6)$
						$\sigma_{A_1(3.6)}$	$\sigma_{\phi_1(3.6)}$	$\sigma_{R_{21}(3.6)}$	$\sigma_{R_{31}(3.6)}$	$\sigma_{\phi_{21}(3.6)}$	$\sigma_{\phi_{31}(3.6)}$
HV1002	1.483 90	245 5153.441	4	0.915 71	0.459 85	0.204 95	4.669 68	0.229 86	0.121 79	4.645 03	3.121 37
						0.003 05	0.014 73	0.015 08	0.015 48	0.072 40	0.127 44
HV1003	1.386 30	245 5144.947	4	0.953 12	0.479 29	0.156 81	4.829 64	0.212 30	0.140 30	4.936 81	2.836 12
						0.003 33	0.020 91	0.021 09	0.020 88	0.110 05	0.168 87
Star ID	log (*P*)	t_0 (JD)	*N*	$S_k(4.5)$	$A_c(4.5)$	$A_1(4.5)$	$\phi_1(4.5)$	$R_{21}(4.5)$	$R_{31}(4.5)$	$\phi_{21}(4.5)$	$\phi_{31}(4.5)$
						$\sigma_{A_1(4.5)}$	$\sigma_{\phi_1(4.5)}$	$\sigma_{R_{21}(4.5)}$	$\sigma_{R_{31}(4.5)}$	$\sigma_{\phi_{21}(4.5)}$	$\sigma_{\phi_{31}(4.5)}$
HV1002	1.483 90	245 5152.041	4	1.336 45	0.508 30	0.216 50	4.634 55	0.220 88	0.135 94	4.211 54	2.921 94
						0.003 30	0.014 93	0.015 34	0.014 65	0.076 10	0.125 36
HV1003	1.386 30	245 5142.933	4	1.188 18	0.602 56	0.161 66	4.589 25	0.182 91	0.175 68	4.636 19	2.196 34
						0.003 64	0.022 25	0.021 98	0.022 19	0.134 88	0.149 87

Notes. This table is available entirely in a machine-readable form in the online journal as supporting information.
Star ID's consisting of four numbers are based on the OGLE-III catalogue.

We used the light-curve data from Macri et al. (2014), who carried out a JHK_s survey of the central ∼18 deg^2 of the LMC using the CPAPIR camera at the Cerro Tololo Inter-American Observatory 1.5-m telescope, operated as part of the SMARTS consortium. The variables, originally identified by OGLE-III (Soszynski et al. 2008) range in period from 1 to 37 d, with an average number of 16 phase points per object. The observations were calibrated by the authors into the 2MASS system. We used 384, 442, 398 light curves in *J*, *H* & K_s, respectively.

We have also used the JHK_s data for 90 Cepheids in the LMC from Persson et al. (2004). These observations were carried out with the 1-m Swope and 2.5-m duPont telescopes at Las Campanas Observatory between 1993 and 1997. These stars have periods in the range of 2 to 134 d and an average of 22 observations per band. These observations were reported using the LCO photometric system, and were transformed into the 2MASS system using the previously referenced relations.

3.3 Mid-infrared wavelengths

We used the 3.6- and 4.5-μm light curves of 37 Galactic and 84 LMC Cepheids obtained by Monson et al. (2012) and Scowcroft et al. (2011), respectively, using *Spitzer* and Infrared Array Camera (IRAC) channels 1 and 2. The variables range in period from 4

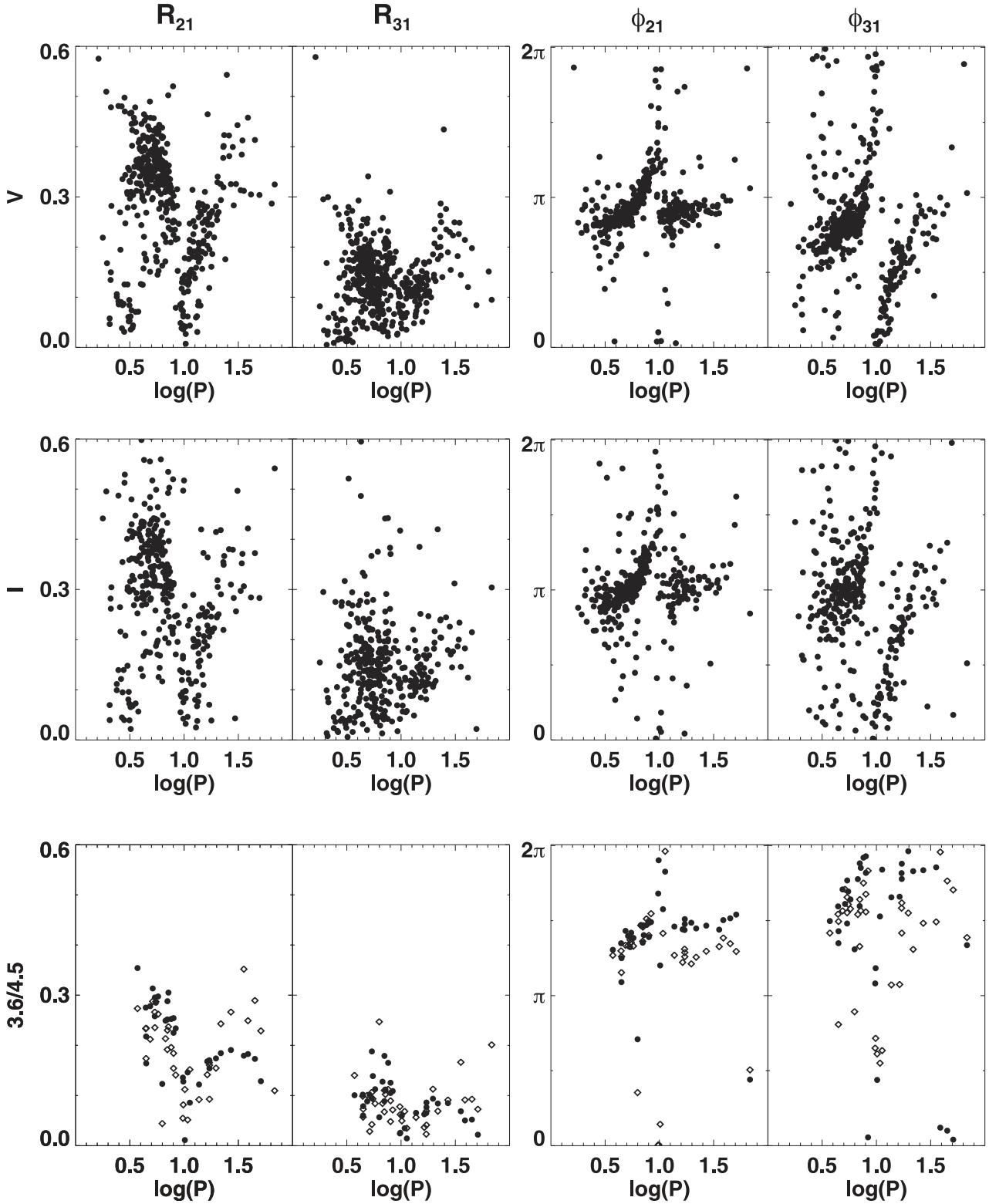

Figure 3. Galactic Cepheid Fourier parameters for the *V* (top row), *I* (middle row) and mid-infrared (bottom row) bands. In the mid-infrared panels, circles and diamonds represent 3.6- and 4.5-μm data, respectively. The first two columns show Fourier amplitude parameters (R_{21} and R_{31}) while the last two represent Fourier phase parameters (ϕ_{21} and ϕ_{31}).

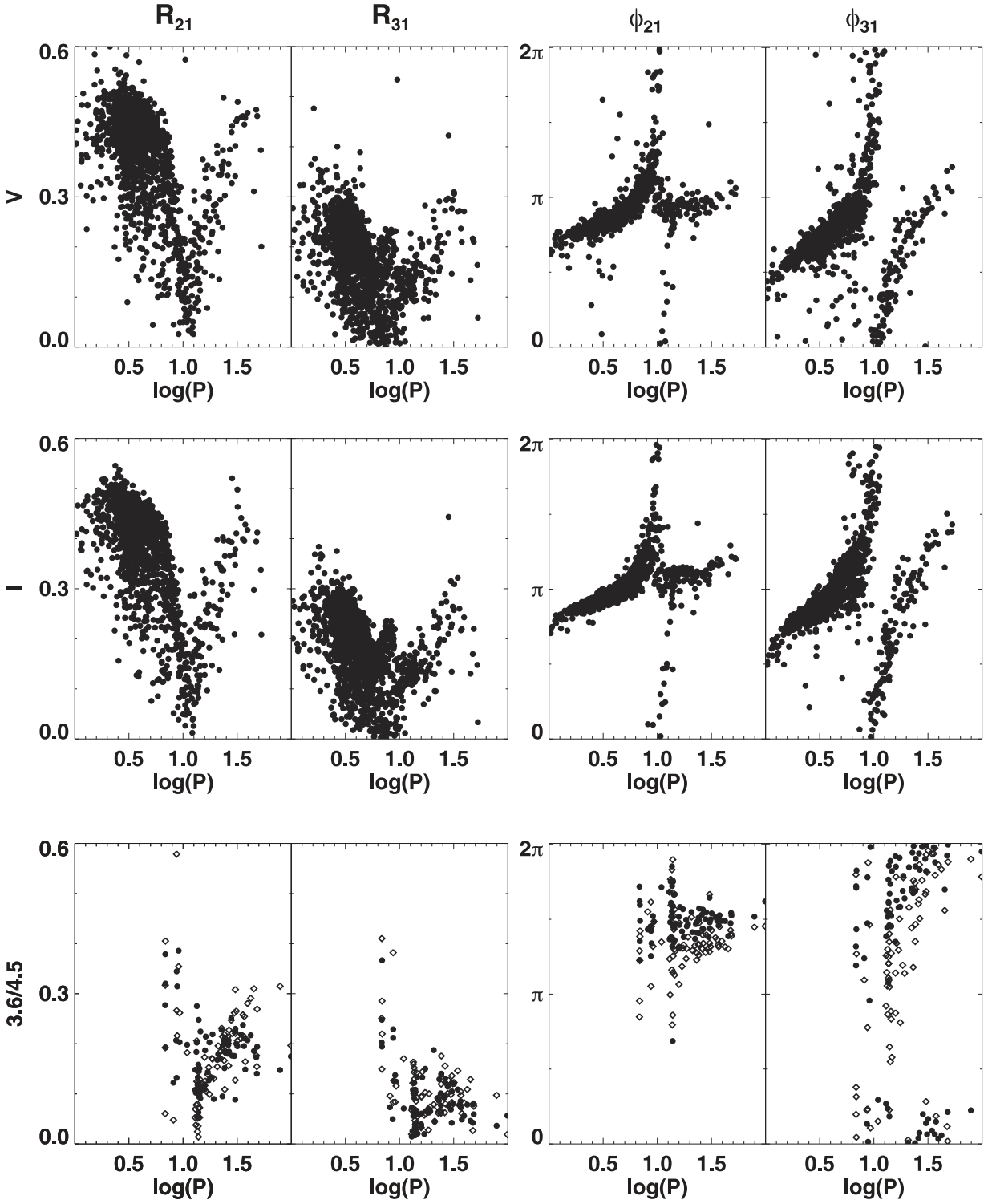

Figure 4. LMC Cepheid Fourier parameters, presented in the same manner as Fig. 3.

to 70 d for the Milky Way and 6 to 140 d for the LMC, and were observed at 24 phase points from 2009 to 2011.

4 FOURIER ANALYSIS OF GALACTIC AND LMC CEPHEIDS

We applied the Fourier decomposition method discussed in Section 2 individually to each Galactic and LMC Cepheid light curve, analysing each bandpass separately. We implemented equation (2) using the IDL MPCURVEFIT routine, varying the order of the fit in each band from 4 to 8. The optimum order of fit (N) was determined using Baart's condition, depending on the residuals for each star (Baart 1982; Deb & Singh 2009). The resulting Fourier coefficients were used to calculate Fourier parameters using equation (3). Fourier-fitted light curves for two Galactic and two LMC Cepheids are shown in Figs 1 and 2, respectively. The Fourier parameters for

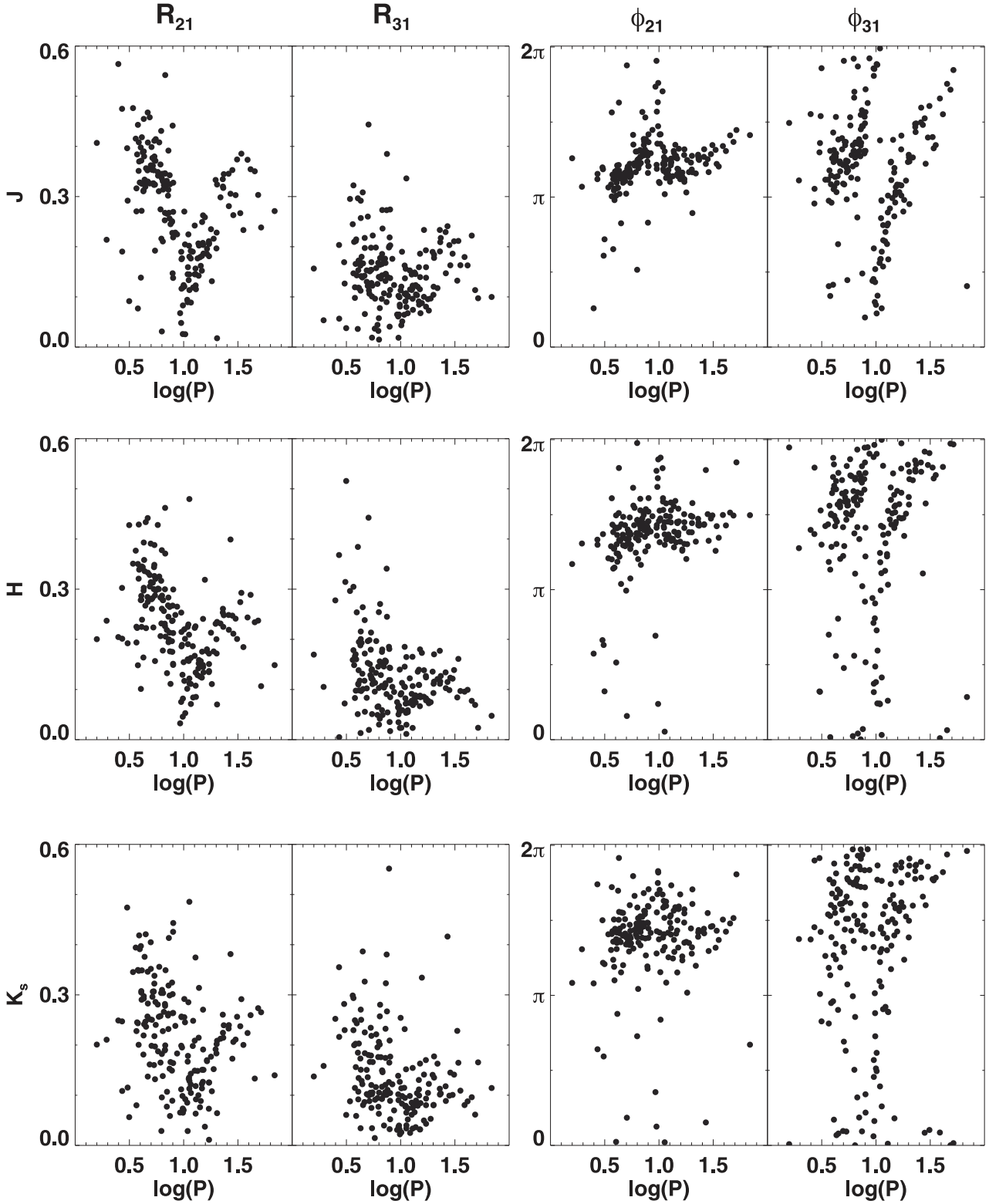

Figure 5. Galactic Cepheid Fourier parameters for the J (top row), H (middle row) and K_s (bottom row) bands, arranged in the column order as Fig. 3.

all variables in all bands are presented in Tables 2 and 3 for Galactic and LMC Cepheids, respectively. In all the figures presented in our paper, the values of the Fourier phase parameter ϕ_{31}, obtained using a sine series, were converted into cosine series by adding a value of π to those given in Tables 2 and 3 (Deb & Singh 2014).

4.1 Optical bands

We have determined the Fourier parameters (R_{21}, R_{31}, ϕ_{21} and ϕ_{31}) of one of the largest samples of Galactic Cepheids at optical wavelengths, with 447 objects in V and 351 in I. These are shown in the top two rows of Fig. 3 as a function of log (P).

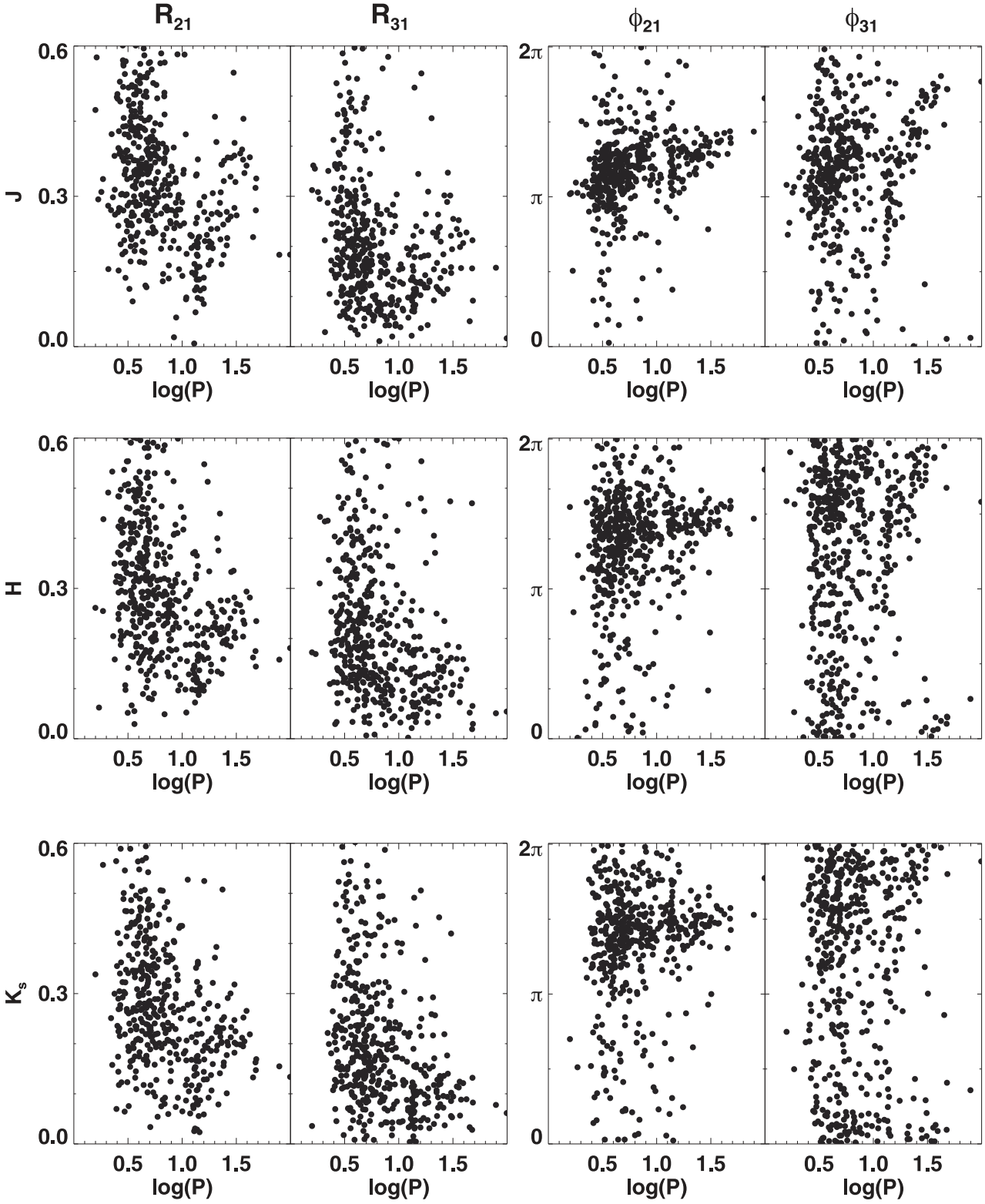

Figure 6. LMC Cepheid Fourier parameters, presented in the same manner as Fig. 5.

The Hertzsprung progression (hereafter HP), indicated by a sharp dip or change in the way the Fourier parameters change with period, is clearly observed for R_{21}, ϕ_{21} and ϕ_{31} in the vicinity of $\log(P) = 1.0$. The centre of this HP seems to be located at slightly shorter period. R_{31} exhibits a flatter minimum that extends over a couple of days in the vicinity of $\log(P) = 1.0$. The uncertainties in the Fourier parameters are very small, given the fairly good phase coverage and number of data points in the light curves.

The top two rows of Fig. 4 show the corresponding analysis for OGLE-III LMC Cepheids in V and I bands. These light curves

have excellent sampling and full phase coverage, thereby yielding very well-determined Fourier parameters that show clear patterns as discussed by Soszynski et al. (2008) and Ulaczyk et al. (2013) in their data release papers.

4.2 Near-infrared bands

Fig. 5 presents the Fourier parameters for 186 Galactic Cepheids that presently have full phase coverage. The HP is clearly observed for all parameters in the vicinity of $\log(P) = 1.0$. We also noticed a more gradual increase of ϕ_{31} for $\log(P) > 1.0$ with increasing wavelength. Since the near-infrared data have a lower number of epochs and poorer phase coverage, the errors in the parameters are larger than at optical bands. The J-band parameters are the best determined ones, with increasing scatter at H and K_s.

Fig. 6 presents the corresponding results for the near-infrared LMC data, including the first-ever Fourier analysis of the light curves from Macri et al. (2014). Since these light curves are not as well sampled as their optical counterparts, we observe more scatter in the Fourier parameters. The better sampled light curves from Persson et al. (2004), which predominantly cover variables with $\log(P) > 1.0$, enable us to clearly see the HP in the J-band Fourier parameters, while the H and K_s panels exhibit greater scatter.

4.3 Mid-infrared bands

The mid-infrared Fourier parameters for Galactic Cepheids are plotted in the bottom row of Fig. 3, showing for the first time the variation of light-curve structure as a function of period at these wavelengths. Even with a smaller number of Cepheids in the sample, the HP is clearly visible for all Fourier parameters. The value of R_{21} displays an abrupt rise from $\log(P) = 1.0$ to a maximum value of $\log(P) = 1.5$ at 4.5 μm, which is not seen at 3.6 μm. Since these light curves have equal phase spacing and the same number of data points, the errors in the parameters are smaller than in their near-infrared counterparts.

The corresponding parameters for LMC Cepheids are displayed in the bottom row of Fig. 4. We observe similar patterns to those exhibited by the Galactic variables.

5 COMPARISON OF FOURIER PARAMETERS

5.1 Fourier amplitude and phase coefficient

We discuss the variation of the first harmonic of amplitude (A_1) and first Fourier phase coefficient (ϕ_1) with period and wavelength. The plots are shown in Figs 7 and 8, for Galactic and LMC Cepheids, respectively. We removed the 2σ outliers in these plots to make the progression visible. At a given period, we observe a decrease in the value of A_1 and an increase in ϕ_1 with increasing wavelength for both Galaxy and LMC. For $1.0 < \log(P) < 1.5$, we find a greater increase in the value of A_1 and decrease in ϕ_1 at optical bands as compared to their infrared counterparts. Also, for $\log(P) > 1.3$, both coefficients show a very small variation and nearly a flat curve at infrared bands. A larger scatter in the value of ϕ_1 is observed for infrared bands.

We note that the variation of light-curve amplitude is essentially similar to A_1 but the variation of phase of maximum light (corresponding to t_0) is not necessarily same as ϕ_1. As the infrared band light curves have larger phase gaps and ϕ_1 depends on the value of t_0, we expect a greater scatter in these bands as observed in Figs 7

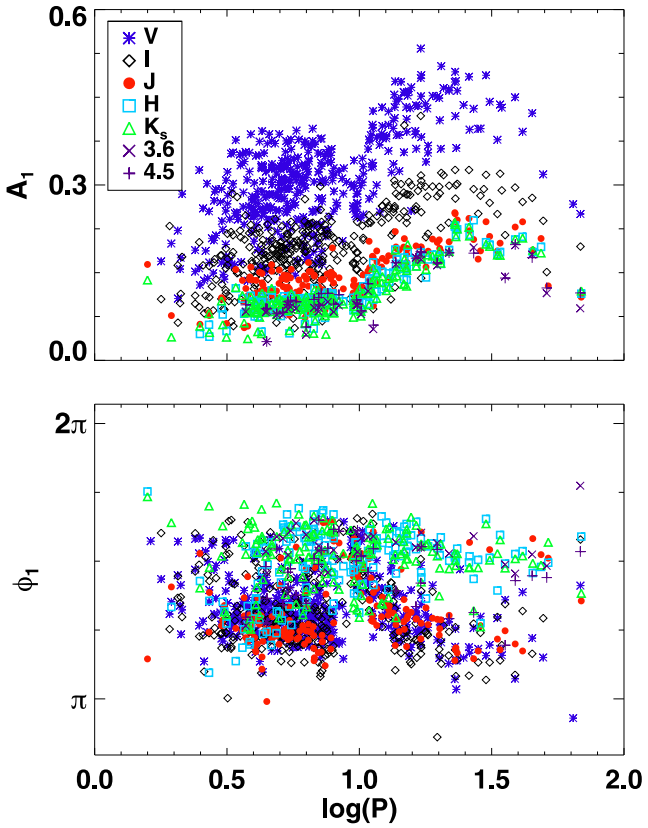

Figure 7. Variation of Fourier amplitude (A_1) and phase (ϕ_1) coefficients for Galactic Cepheids in multiple bands.

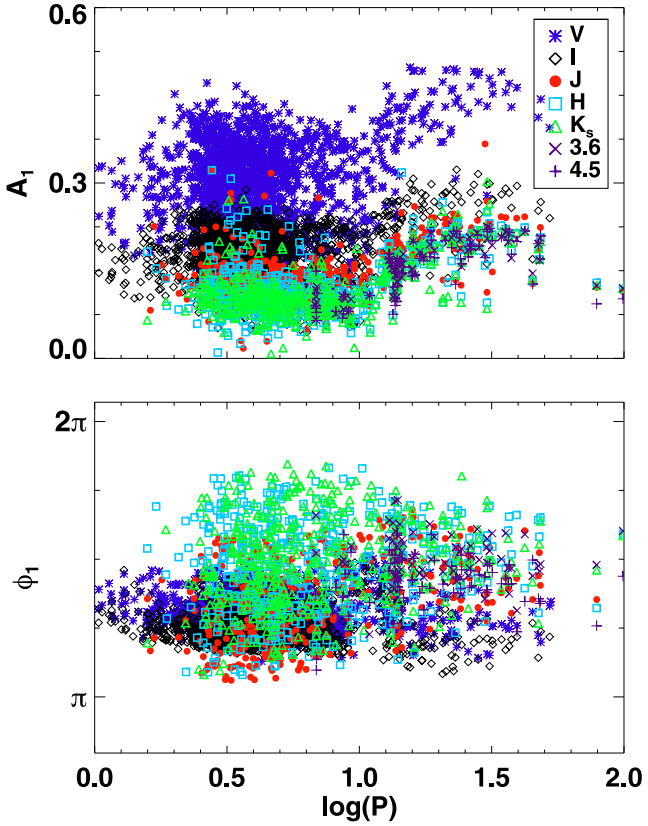

Figure 8. Same as Fig. 7, but for LMC Cepheids.

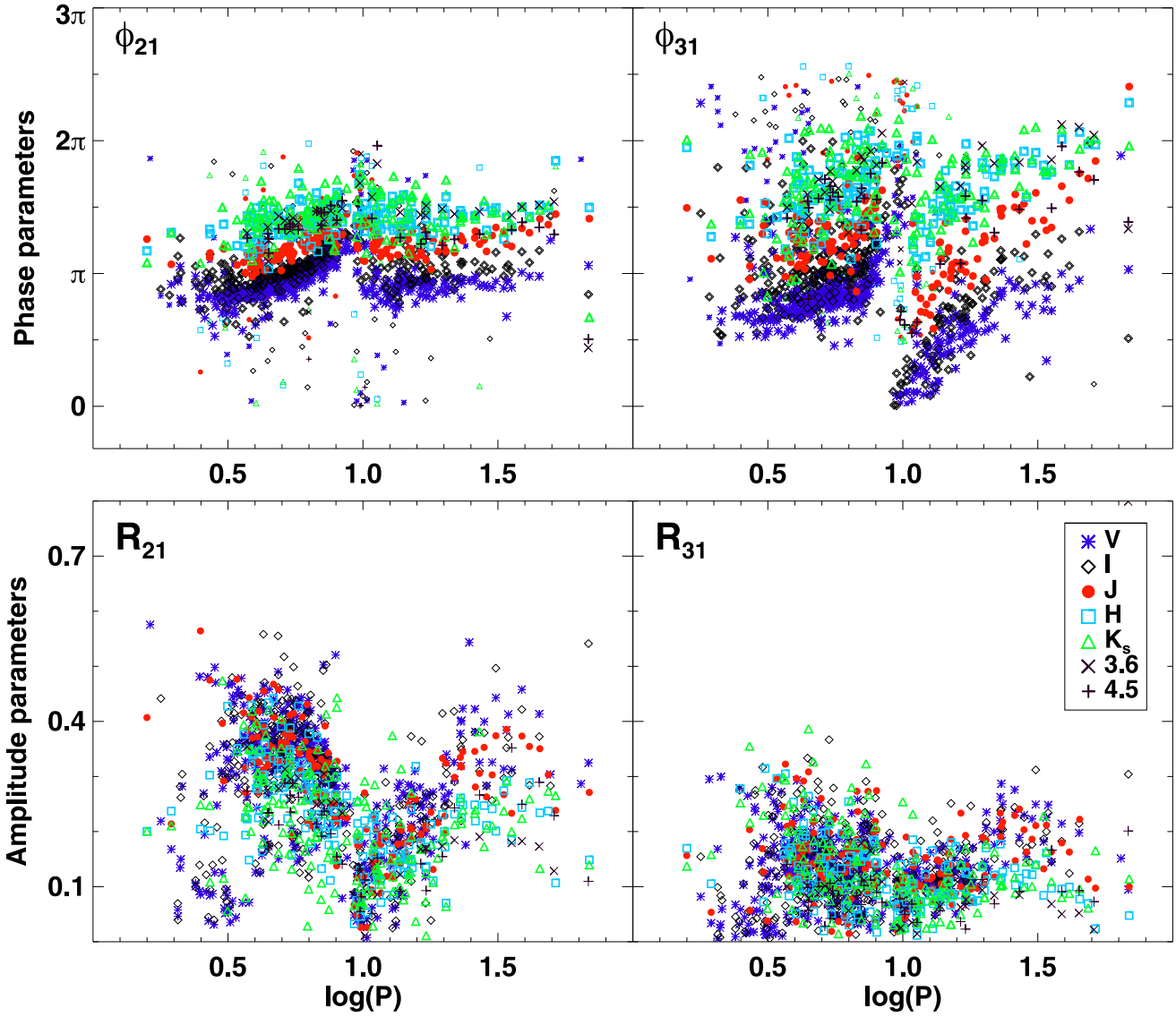

Figure 9. Fourier parameters plotted against log (*P*) for Galactic Cepheids, in multiple bands. Some phase parameters have been shifted by 2π for plotting purposes. The outliers in phase parameters for each band are shown using smaller symbols.

and 8. For example, in Fig. 1 the *J*-band light curve for *T MON* show a flatter maxima, which also causes an uncertainty in the determination of exact phase corresponding to maximum light. The phase difference at maximum light for Cepheids in the Galaxy in multiple bands is discussed in Madore & Freedman (1991) while $\Delta\phi_{\rm max}(I$ versus $JHK_{\rm s})$ for first results of LMC Cepheids used in our analysis is discussed in Macri et al. (2014). This phase difference at maximum light and its variation with wavelength is related to period–colour relations at maximum light discussed in Bhardwaj et al. (2014).

We also emphasize that the coefficients ϕ_i are not independent of time translation and this is the reason phase parameters (ϕ_{i1}) are preferred to study the light-curve structure (Simon & Lee 1981). These are perhaps more easily compared between data sets where the initial epoch of observation is not known. The variation of phase parameters with period and wavelength will be discussed in the following subsections.

5.2 Individual Fourier parameters

In order to analyse the variation of Fourier parameters as a function of wavelength and period, we overplotted the phase and amplitude parameters using different symbols and colours for each band, and removed 2σ outliers to make the HPs more easily visible. Figs 9 and 10 present the parameters for the Galactic and LMC samples, respectively.

We observed a clear trend in the ϕ_{21} and ϕ_{31} for both Galactic and LMC Cepheids that become larger with increasing wavelength at fixed period. For these phase parameters, the outliers are shown using smaller symbols for all bands to avoid any loss of features near the centre of the HP. These outliers follow the same trend as all points and the features of the plot are not affected by varying the degree of outlier removal. No clear trend with wavelength at fixed period is seen for the R_{21} and R_{31}. Considering long-period (log $(P) > 1.0$) variables, the amplitude parameters can be separated into two groups; one for *VIJ* and another for the longer wavelengths.

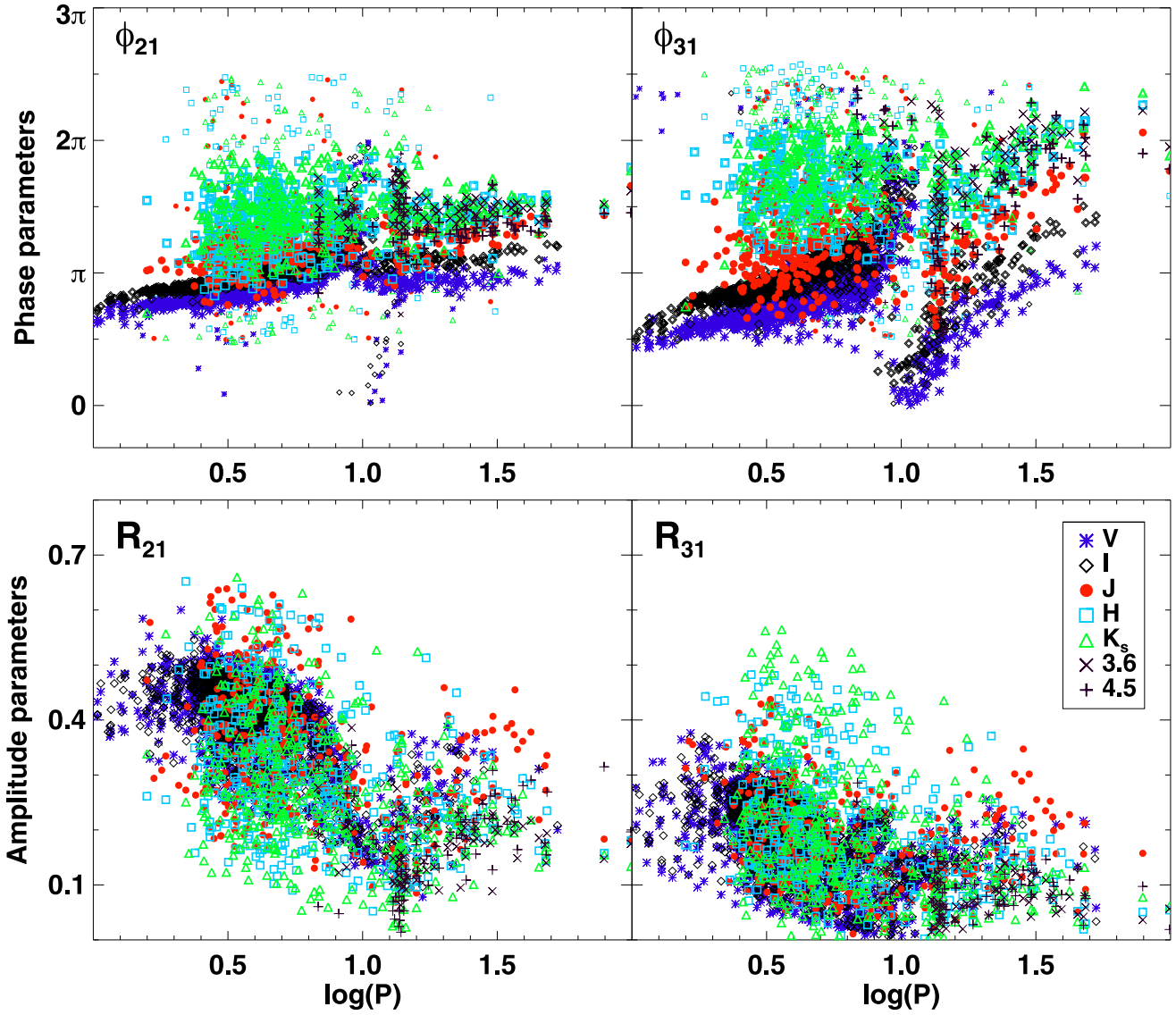

Figure 10. Same as Fig. 9, but for LMC Cepheids.

Furthermore, the latter bands exhibit a slight drop after $\log(P) = 1.3$ ($P = 20$ d) while the former ones seem to rise. We also observed a turnover in amplitude parameters around $\log(P) = 1.5$ that varies with wavelength. Since we have removed 2σ outliers in this figure, the Galactic data show more clearly that the centre of the HP occurs slightly before $\log(P) = 1.0$ for all parameters while it remains at $\log(P) = 1.0$ for the LMC variables.

5.3 Mean Fourier parameters

In order to clearly discern any wavelength-dependent variation in Fourier parameters, we computed sliding mean values with steps of 0.04 dex in $\log(P)$ and a bin width of 0.2 dex. We found these values yielded the least amount of scatter between consecutive points after significant experimentation with various choices.

Fig. 11 shows the result for Galactic Cepheids. The increase in phase parameters with increasing wavelength becomes more clear and distinct. We also see clearly the decrease in amplitude parameters with increasing wavelength at a given period. Both R_{21} and R_{31} exhibit a sharp rise beyond $\log(P) = 0.9$ to a peak around $\log(P) = 1.4$ and a decrease around $\log(P) = 1.7$. This behaviour is more pronounced for *VIJ* than for the redder bands. The minimum is more pronounced for R_{21}, while R_{31} shows a shallower minimum. There is also a hint of change in the behaviour of the parameters for $\log(P) > 1.8$. This may be connected to the properties of ultralong period Cepheids (Ngeow et al. 2013). Considering the short-period variables, both parameters exhibit maximum values around $\log(P) = 0.6$. The increased scatter for $\log(P) < 0.5$ may be due to a combination of a smaller number of stars and contamination by first overtone pulsators.

The corresponding plots for LMC Cepheids are presented in Fig. 12. The same patterns present in Galactic Cepheids are also seen in this sample. The data suggest a separation between optical and infrared Fourier phase parameters for $\log(P) < 0.5$, which may extend to R_{21} but is not visible in R_{31}. Figs 11 and 12 were used to determine the average behaviour of the Fourier parameters with wavelength at given period. Flat sections in these plots do occur when Fourier parameters oscillate from a high to low value or vice versa, particularly when we are near the centre of the HP. For example, the flat section in R_{31} for LMC Cepheids in Fig. 12

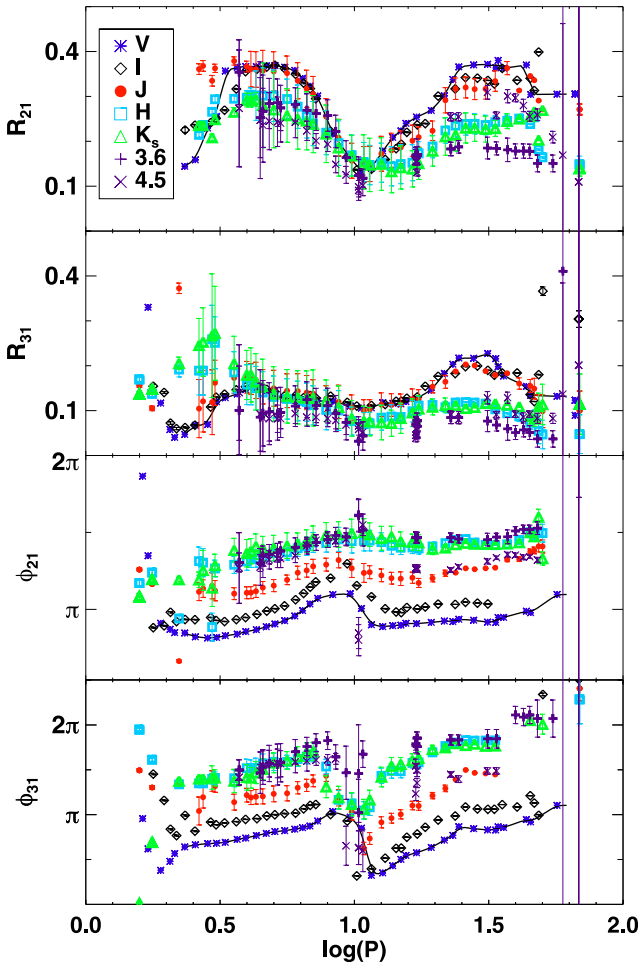

Figure 11. Mean Fourier Parameters for Galactic Cepheids. Some phase parameters have been shifted by 2π for plotting purposes. The error bars represent the standard error in the mean values.

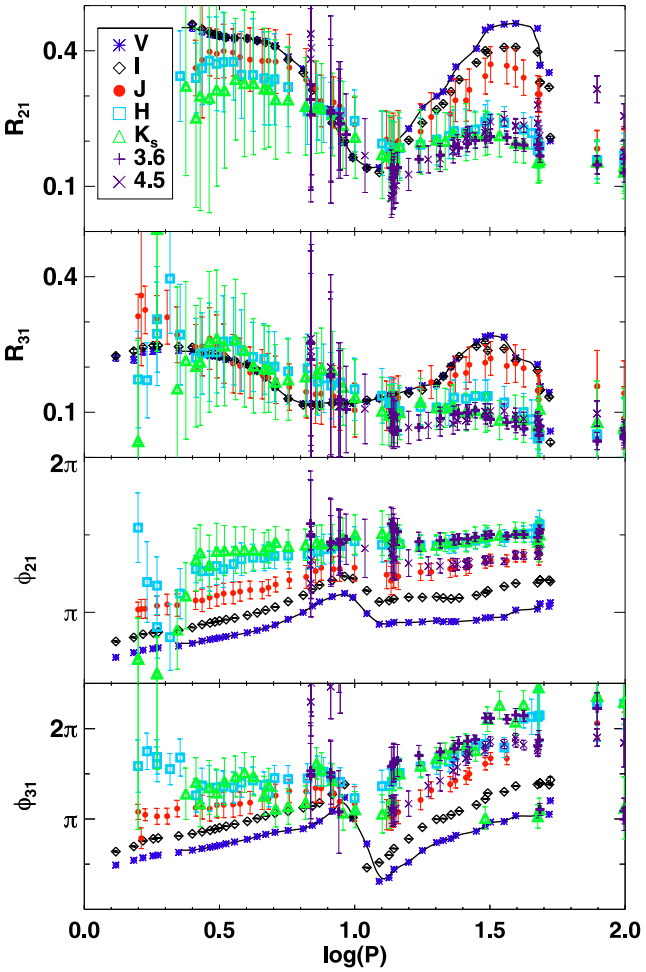

Figure 12. Same as Fig. 12, but for LMC Cepheids.

is due to the R_{31} clump at periods $0.8 < \log(P) < 1.0$ observed at optical bands in Fig. 4. However, such plots do provide evidence that the HP is most dramatic at shorter wavelengths and in R_{21} and ϕ_{21} parameters (Simon & Lee 1981).

We quantitatively analysed the progression of mean Fourier parameters with period and wavelength by calculating the change in mean parameter values (binned every 0.2 dex in $\log(P)$) across two bands. We restricted the analysis to $0.5 < \log(P) < 1.5$ because this period range provides smooth progressions for each parameter with reduced scatter. The result of this analysis is given in Table 4, for both the Galaxy and LMC. Comparing the *V*- and *I*-band results, we observed a negligible change in amplitude parameters while there was a nearly constant offset in phase parameters for all period bins except for the one centred at $\log(P) = 1.0$. Comparing the optical to near-infrared results, the change in amplitude parameters is small around $\log(P) = 1.0$, increasing slowly up to $\log(P) = 1.3$ and sharply afterwards. The change in the values of amplitude parameters when comparing wavelengths shorter and longer than *J* is greatest for $1.3 < \log(P) < 1.5$. In the case of the phase parameters, we observed a similar and significant difference in most of the periods bins. The comparisons of *H* to K_s and 3.6–4.5 μm exhibit a small change in amplitude parameters and a large scatter in the phase parameters. We note that $\Delta\phi$ values for (V, K_s), (J, K_s), (H, K_s) increase as a function of wavelength, while ΔR values decrease as a function of wavelength for $0.5 < \log(P) < 1.5$.

5.4 Skewness and acuteness parameters

We also observed the variation of skewness (S_k) and acuteness (A_c) parameters following the work of Stellingwerf & Donohoe (1986, 1987) and Bono et al. (2000). Stellingwerf & Donohoe (1987) defined skewness as the ratio of the phase duration of the descending branch to the phase duration of the rising branch. They defined acuteness as the ratio of the phase duration during which the magnitude is fainter than the median magnitude to the phase duration during which it is brighter than median magnitude. If $\phi_{\rm min}$ and $\phi_{\rm max}$ are the phases corresponding to the extremum of the rising branch, the phase duration of the rising branch is $\phi_{\rm rb} = \phi_{\rm max} - \phi_{\rm min}$. Similarly, following Bono et al. (2000), we defined the median magnitude to be, $m_{\rm med} = 0.5 \times (m_{\rm max} + m_{\rm min})$ and $\phi_{\rm fw}$ as the full width at half-maximum of the light curve, which is equivalent to phase duration of brighter than average light. Hence,

$$S_k = \frac{1}{\phi_{\rm rb}} - 1; \quad A_{\rm c} = \frac{1}{\phi_{\rm fw}} - 1.$$

The skewness is a measure of left/right asymmetry and it decreases when the slope of the rising branch becomes flatter while acuteness is a measure of the top-down asymmetry of the light curve and it decreases when the shape changes from sawtooth to

Table 4. Variation of mean Fourier parameters determined as a difference in multiple bands in each period bin of $\log(P) = 0.2$.

$\log(P)$	$\Delta R_{21}(V, I)$	$\Delta R_{21}(V, K_s)$	$\Delta R_{21}(J, K_s)$	$\Delta R_{21}(H, K_s)$	$\Delta R_{21}(3.6, K_s)$	$\Delta R_{21}(3.6, 4.5)$
			Galaxy			
0.5–0.7	0.031 ± 0.002	0.082 ± 0.064	0.081 ± 0.076	0.018 ± 0.081	0.020 ± 0.097	0.047 ± 0.149
0.7–0.9	0.005 ± 0.002	0.101 ± 0.059	0.071 ± 0.070	0.016 ± 0.073	0.033 ± 0.070	0.045 ± 0.051
0.9–1.1	−0.003 ± 0.001	−0.001 ± 0.040	0.002 ± 0.053	0.003 ± 0.057	0.004 ± 0.054	0.042 ± 0.043
1.1–1.3	0.023 ± 0.001	0.080 ± 0.034	0.047 ± 0.041	0.011 ± 0.042	0.020 ± 0.038	0.018 ± 0.020
1.3–1.5	0.022 ± 0.000	0.127 ± 0.002	0.090 ± 0.002	0.012 ± 0.002	−0.038 ± 0.015	−0.084 ± 0.018
			LMC			
0.5–0.7	0.001 ± 0.005	0.105 ± 0.108	0.066 ± 0.124	0.032 ± 0.130	−0.318 ± 0.108	0.000 ± 0.000
0.7–0.9	0.007 ± 0.005	0.058 ± 0.098	0.047 ± 0.121	0.003 ± 0.120	0.002 ± 0.191	−0.066 ± 0.356
0.9–1.1	0.003 ± 0.004	−0.057 ± 0.080	0.032 ± 0.104	0.021 ± 0.105	−0.004 ± 0.145	−0.015 ± 0.170
1.1–1.3	0.026 ± 0.003	0.060 ± 0.063	0.029 ± 0.078	0.011 ± 0.081	−0.039 ± 0.074	0.038 ± 0.055
1.3–1.5	0.044 ± 0.003	0.163 ± 0.046	0.099 ± 0.061	0.016 ± 0.059	−0.022 ± 0.049	−0.008 ± 0.028
$\log(P)$	$\Delta R_{31}(V, I)$	$\Delta R_{31}(V, K_s)$	$\Delta R_{31}(J, K_s)$	$\Delta R_{31}(H, K_s)$	$\Delta R_{31}(3.6, K_s)$	$\Delta R_{31}(3.6, 4.5)$
			Galaxy			
0.5–0.7	−0.006 ± 0.001	−0.028 ± 0.061	−0.005 ± 0.072	−0.016 ± 0.076	−0.074 ± 0.097	−0.012 ± 0.125
0.7–0.9	−0.007 ± 0.002	−0.002 ± 0.060	0.011 ± 0.071	−0.012 ± 0.074	−0.021 ± 0.075	0.021 ± 0.051
0.9–1.1	−0.007 ± 0.001	0.025 ± 0.040	0.022 ± 0.049	−0.006 ± 0.051	−0.021 ± 0.057	−0.003 ± 0.046
1.1–1.3	−0.005 ± 0.001	0.034 ± 0.031	0.035 ± 0.039	0.007 ± 0.040	−0.017 ± 0.035	0.027 ± 0.018
1.3–1.5	0.020 ± 0.000	0.099 ± 0.002	0.078 ± 0.002	0.005 ± 0.002	−0.028 ± 0.013	−0.015 ± 0.016
			LMC			
0.5–0.7	−0.001 ± 0.005	−0.022 ± 0.104	−0.021 ± 0.119	0.012 ± 0.130	−0.215 ± 0.104	0.000 ± 0.000
0.7–0.9	0.003 ± 0.005	−0.061 ± 0.090	−0.038 ± 0.111	−0.001 ± 0.117	0.034 ± 0.210	−0.010 ± 0.292
0.9–1.1	−0.000 ± 0.004	−0.037 ± 0.085	−0.038 ± 0.108	−0.002 ± 0.112	−0.040 ± 0.152	0.015 ± 0.177
1.1–1.3	0.006 ± 0.003	0.050 ± 0.064	0.034 ± 0.080	0.015 ± 0.083	−0.039 ± 0.075	−0.026 ± 0.055
1.3–1.5	0.031 ± 0.003	0.141 ± 0.042	0.089 ± 0.057	0.024 ± 0.056	−0.010 ± 0.046	0.008 ± 0.028
$\log(P)$	$\Delta\phi_{21}(V, I)$	$\Delta\phi_{21}(V, K_s)$	$\Delta\phi_{21}(J, K_s)$	$\Delta\phi_{21}(H, K_s)$	$\Delta\phi_{21}(3.6, K_s)$	$\Delta\phi_{21}(3.6, 4.5)$
			Galaxy			
0.5–0.7	−0.303 ± 0.005	−1.673 ± 0.257	−0.836 ± 0.285	−0.192 ± 0.310	−0.203 ± 0.321	0.115 ± 0.422
0.7–0.9	−0.331 ± 0.006	−1.460 ± 0.250	−0.614 ± 0.283	−0.118 ± 0.311	−0.145 ± 0.310	0.080 ± 0.232
0.9–1.1	−0.499 ± 0.009	−1.466 ± 0.274	−0.709 ± 0.331	−0.140 ± 0.366	0.098 ± 0.427	0.827 ± 0.392
1.1–1.3	−0.308 ± 0.004	−1.691 ± 0.194	−0.753 ± 0.228	−0.096 ± 0.239	0.083 ± 0.225	0.639 ± 0.129
1.3–1.5	−0.354 ± 0.002	−1.554 ± 0.007	−0.524 ± 0.009	0.057 ± 0.010	0.128 ± 0.092	0.586 ± 0.104
			LMC			
0.5–0.7	−0.356 ± 0.014	−1.679 ± 0.412	−0.843 ± 0.450	−0.231 ± 0.495	−4.434 ± 0.412	0.000 ± 0.000
0.7–0.9	−0.350 ± 0.017	−1.329 ± 0.353	−0.600 ± 0.423	−0.169 ± 0.465	0.175 ± 0.963	0.658 ± 1.120
0.9–1.1	−0.399 ± 0.023	−1.346 ± 0.398	−0.608 ± 0.472	−0.138 ± 0.494	−0.070 ± 0.672	0.092 ± 0.863
1.1–1.3	−0.495 ± 0.016	−1.665 ± 0.399	−0.711 ± 0.478	−0.088 ± 0.510	0.193 ± 0.495	0.531 ± 0.532
1.3–1.5	−0.498 ± 0.010	−1.592 ± 0.207	−0.518 ± 0.257	−0.026 ± 0.269	0.031 ± 0.232	0.505 ± 0.151
$\log(P)$	$\Delta\phi_{31}(V, I)$	$\Delta\phi_{31}(V, K_s)$	$\Delta\phi_{31}(J, K_s)$	$\Delta\phi_{31}(H, K_s)$	$\Delta\phi_{31}(3.6, K_s)$	$\Delta\phi_{31}(3.6, 4.5)$
			Galaxy			
0.5–0.7	−0.634 ± 0.010	−2.251 ± 0.386	−0.823 ± 0.467	0.193 ± 0.501	0.169 ± 0.722	0.082 ± 0.669
0.7–0.9	−0.621 ± 0.013	−2.321 ± 0.329	−0.812 ± 0.392	0.057 ± 0.417	0.272 ± 0.540	0.293 ± 0.574
0.9–1.1	0.418 ± 0.012	−1.065 ± 0.396	−0.753 ± 0.486	−0.091 ± 0.512	1.197 ± 1.012	1.747 ± 1.104
1.1–1.3	−0.591 ± 0.007	−3.377 ± 0.235	−1.673 ± 0.284	−0.121 ± 0.329	0.704 ± 0.330	1.197 ± 0.321
1.3–1.5	−0.700 ± 0.002	−3.042 ± 0.012	−1.104 ± 0.014	0.116 ± 0.017	0.198 ± 0.178	1.229 ± 0.211
			LMC			
0.5–0.7	−0.633 ± 0.027	−1.834 ± 0.680	−0.557 ± 0.787	0.018 ± 0.826	−4.311 ± 0.679	0.000 ± 0.000
0.7–0.9	−0.678 ± 0.032	−1.425 ± 0.587	−0.151 ± 0.760	0.363 ± 0.776	0.390 ± 1.410	3.220 ± 1.748
0.9–1.1	−0.175 ± 0.036	−1.023 ± 0.609	0.047 ± 0.782	0.521 ± 0.785	−0.579 ± 1.298	0.892 ± 1.699
1.1–1.3	−0.791 ± 0.022	−2.490 ± 0.592	−0.687 ± 0.720	0.457 ± 0.781	0.951 ± 0.852	1.561 ± 0.772
1.3–1.5	−0.819 ± 0.015	−1.691 ± 0.381	0.304 ± 0.447	0.640 ± 0.504	0.392 ± 0.444	−0.318 ± 0.342

flat-topped (Bono et al. 2000). For observed stars, the S_k is generally greater than unity while for symmetric light curves both parameters attain a value close to 1. Since, both skewness and acuteness parameters are a function of phase durations, we use equation (2) to obtain 1000 data points per light curve to determine an accurate value of ϕ_{rb} and ϕ_{fw}. The variation of S_k and A_c with period and wavelength is shown in Figs 13 and 14 for the Galaxy and LMC, respectively. At a fixed period, we find that the value of

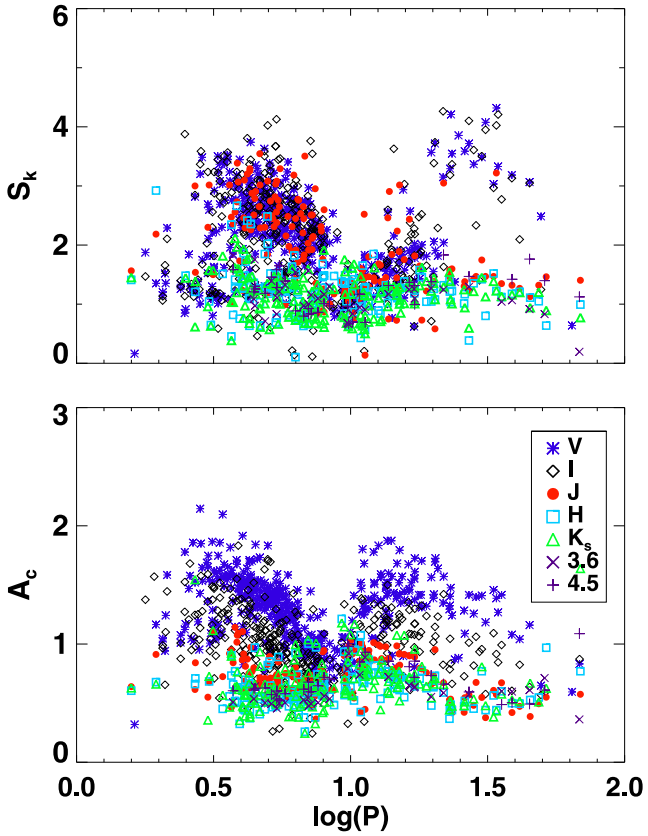

Figure 13. Variation of skewness (S_k) and acuteness (A_c) parameter against log (P) for Galactic Cepheids.

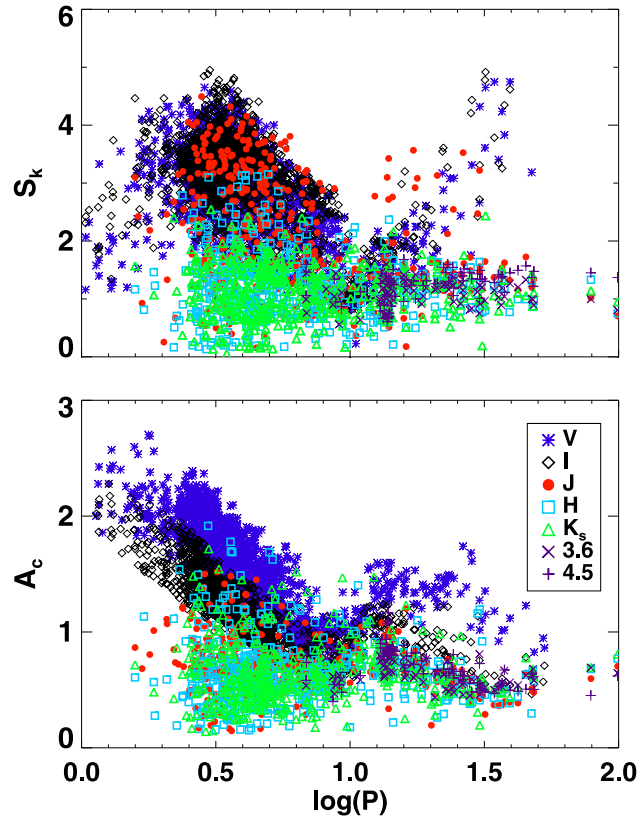

Figure 14. Same as Fig. 13, but for LMC Cepheids.

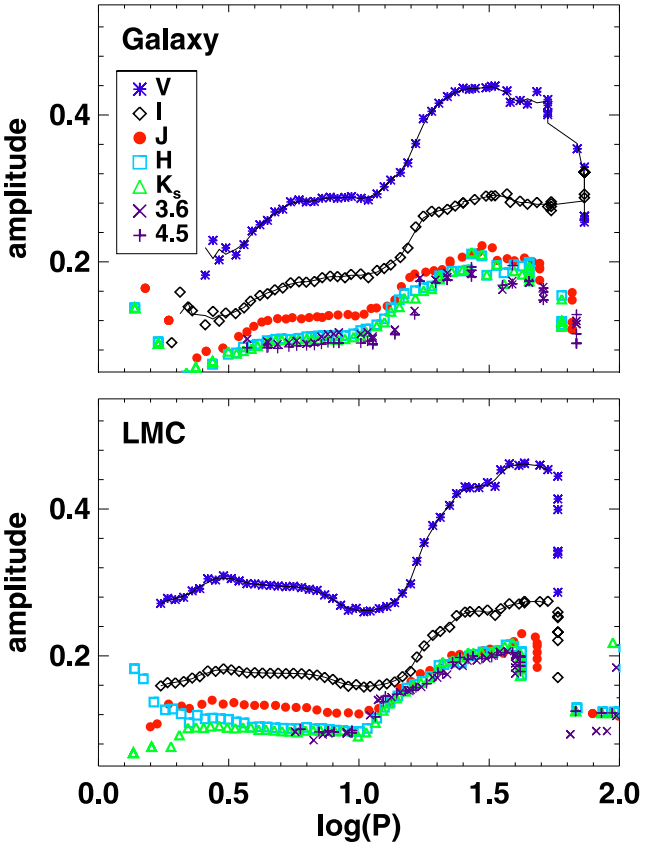

Figure 15. Variation of the mean of light-curve amplitudes in multiple bands with period for Galactic and LMC Cepheids.

S_k and A_c decreases with wavelength. Also, the separation in the values of both parameters for wavelengths shorter/longer than J band is clearly visible for Cepheids having $\log(P) > 1.3$. This behaviour is similar to that of mean Fourier parameters discussed in the previous subsection. As the light curves from optical to infrared bands become more sinusoidal and flat-topped, both the parameters are generally expected to decrease with wavelength. However, the Cepheids having period in the vicinity of 10 d are more symmetric as both parameters attain a value close to unity. We emphasize that the skewness/acuteness parameters are the functions of light-curve shape similar to Fourier parameters so either set can be used to see the variation as they are not independent of each other.

6 THE VARIATION OF THE HP WITH WAVELENGTH

We also observed the variation of mean of light-curve amplitudes with period and wavelength. We apply sliding mean calculations to determine the mean amplitudes similar to mean Fourier parameters. The variation of mean amplitudes at multiple bands for both Galactic and LMC Cepheids is shown in Fig. 15. The mean amplitudes decrease with increasing wavelengths. The amplitudes in the optical bands show a sharp rise for periods $1.0 < \log(P) < 1.5$ as compared to infrared bands.

The mean parameter plots for both Galactic and LMC Cepheids provide evidence for clearly visible trends that could be fit using functional forms. We therefore reduced the step size in the sliding mean calculation to 0.02 in $\log(P)$ with the same bin width of

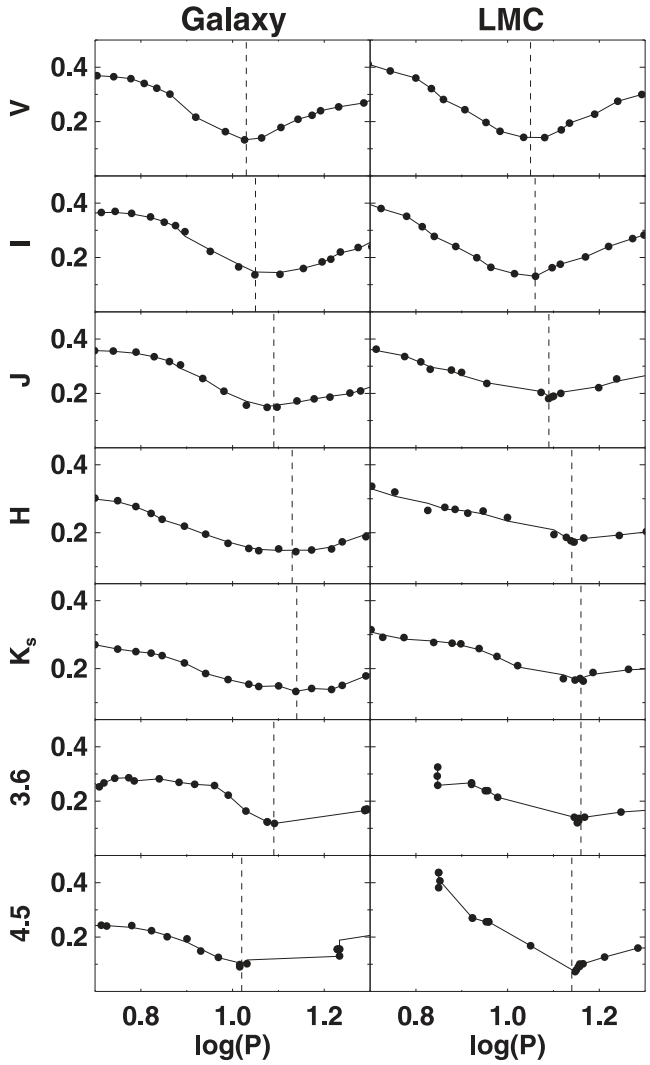

Figure 16. Functional fits to mean Fourier amplitude parameter (R_{21}) in multiple bands, used to determine the central period of HP. The dashed vertical line represents the central period of HP in each band. Similarly, functional fits were also applied to mean light-curve amplitudes to obtain the centre of HP.

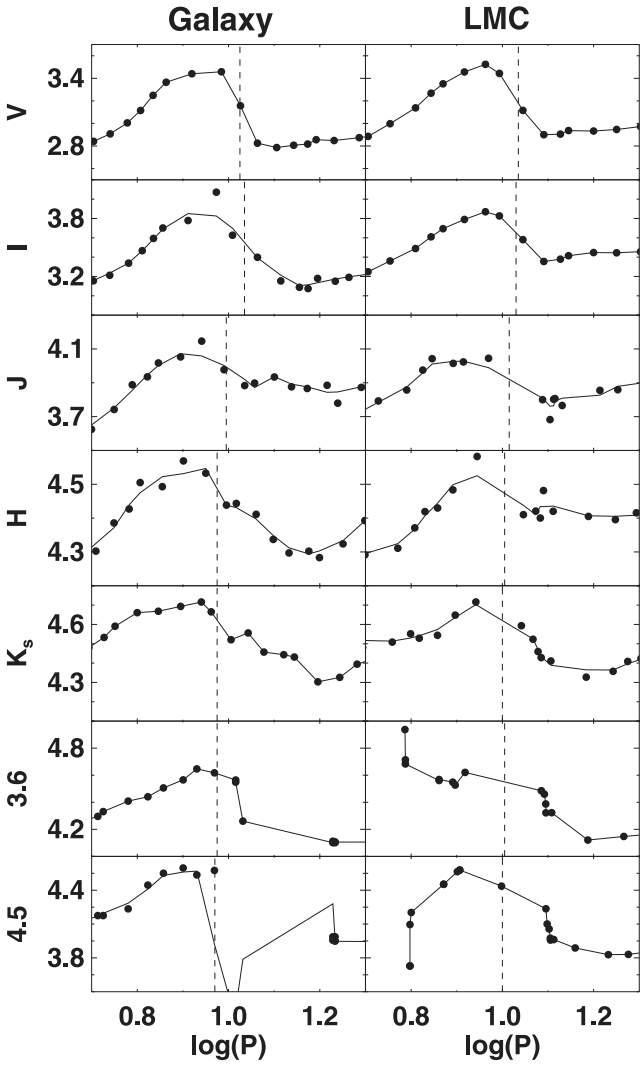

Figure 17. Functional fits to mean Fourier phase parameter (ϕ_{21}) in multiple bands, used to determine the central period of HP. The dashed vertical line represents the central period of HP in each band. Similarly, functional fits were also applied to ϕ_{31} to obtain the centre of HP.

$\log(P) = 0.2$ and fit polynomials of varying degrees. These were then interpolated to obtain values every 0.01 dex. We have presented the functional fit to *V*-band parameters in Figs 11, 12 and 15. We also provide functional fits to multiple band Fourier amplitude parameter (R_{21}) and Fourier phase parameter (ϕ_{21}). These plots will be used to determine the central period of HP, and are shown in Figs 16 and 17. Similar functional fits were also applied to light-curve amplitudes and ϕ_{31} parameter to determine central period of HP.

Following the work of Bono et al. (2000), we determine the central period of HP using light -curve amplitudes. However, we do not observe a sharp minima around $\log(P) = 1.0$ but we also note that both theoretical light and velocity curve display a flatter minima in Bono et al. (2000). The variation of the central period of the HP determined using the light-curve amplitudes is presented in the top panel of Fig. 18. For optical wavelengths, we find that the central period of the HP is at $\log(P) = 1.04$ for *V* band and $\log(P) = 1.03$ for *I* band, in the LMC. These results are in good agreement with the theoretical prediction of $\log(P) = 1.051 \pm 0.018$ by Bono et al. (2000).

We determined the minimum values of R_{21} as a function of wavelength for each sample – these are given in the second panel of Fig. 18. The results argue for a clear trend in the central period of the HP, with the central value increasing with wavelength. For Galactic data at wavelengths longer than K_s, the central period of the HP shifts towards shorter periods. The increased scatter at mid-infrared wavelengths is expected as there are not enough stars in those bands, specially in the vicinity of 10 d. We find that the central period of HP is at $\log(P) = 1.05$ for *V* band and $\log(P) = 1.06$ for *I* band, in the LMC. Again, these results are in excellent agreement with those predicted using theoretical light curves (Bono et al. 2000) and obtained using Fourier parameters (Welch et al. 1997). However, we emphasize that the results of Bono et al. (2000) are obtained using the amplitudes of light and velocity curves while our results are obtained using Fourier amplitude parameter. So the central period of HP determined using the two methods are different

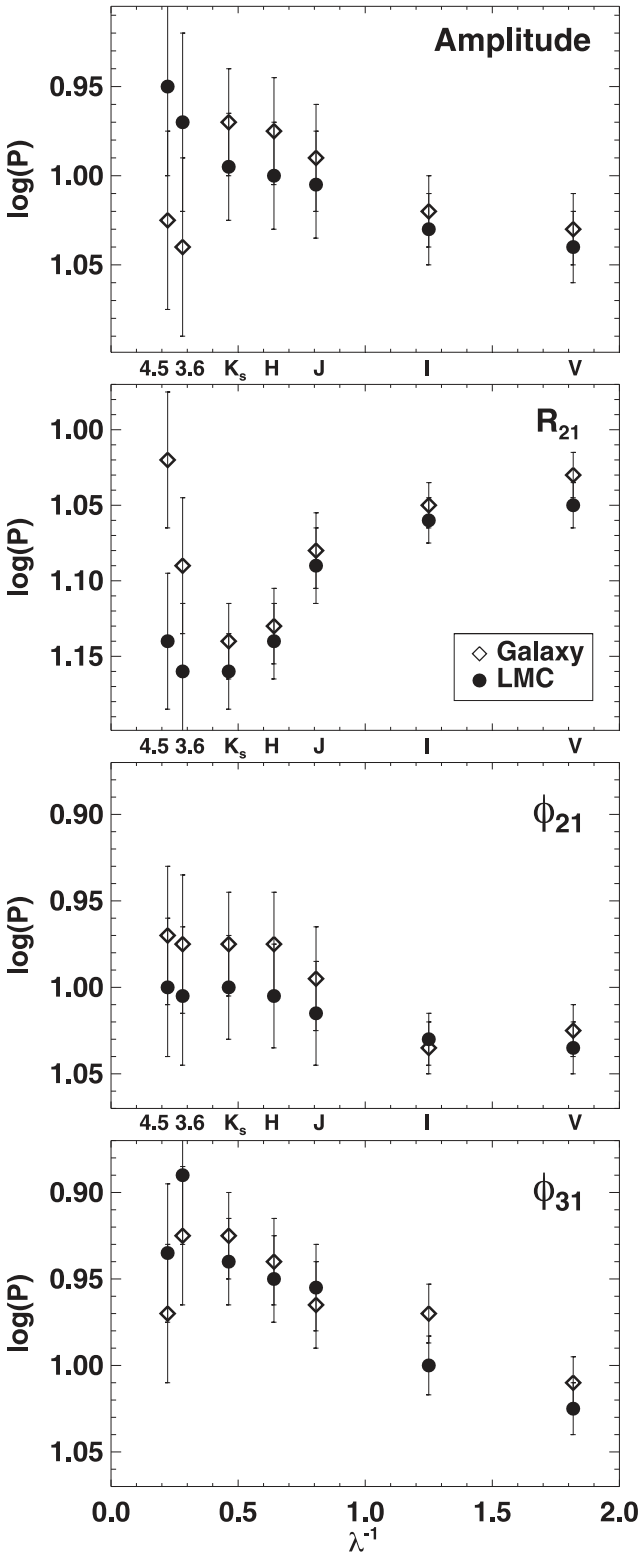

Figure 18. Variation of central period of HP with wavelength for amplitude and Fourier parameters R_{21}, ϕ_{21} and ϕ_{31}. The error bars represent the maximum possible deviation from the median value with different degree of polynomials.

but the agreement in these two results is very interesting. We do not plot the corresponding values for R_{31} since the data imply that this parameter seems to be less sensitive to the bump progression and a shallow minimum is observed in Fig. 12.

In the case of phase parameters, the break in the centre of the HP required a slightly different approach. We fit two polynomials to the points on each side of $\log(P) = 1.0$, restricting the range to ± 0.2 dex from that value. We then estimated the maximum value before 10 d and the minimum value just after 10 d. We linearly interpolated across these extrema and took the mid-point of the resulting line to be the centre of the HP. We do not observe sharp minima after 10 d at infrared bands due to smaller amplitudes and larger scatter in phase parameters, as shown in Fig. 17. However, there is a small but significant drop in the value of ϕ_{21} in the vicinity of 10 d. In such cases, where the minima is flat or extended towards a longer period, we have chosen the first point lying on the functional fit as minima after 10 d. We consider the mid-point of these extremums obtained from functional fits as the centre of HP. The results obtained from the fits to phase parameters are shown in the bottom two panels of Fig. 18. Again, there seems to be a clear trend in the value of the centre of the HP, but now decreasing with increasing wavelength. In the case of ϕ_{21}, the central period occurs at $\log(P) \sim 1.04$ in the optical bands for both Galaxy and LMC, consistent with the previous determination of $\log(P) = 1.049 \pm 0.031$ by Welch et al. (1997).

We have also observed a slight difference in the central period of the HP for the Galaxy and LMC in each parameter. This difference is most likely due to metallicity differences between the two galaxies. As seen in Fig. 18, the greatest disparity in the central period of the HP happens longwards of K_s for amplitude and R_{21} and beyond J for ϕ_{21}. No significant difference is seen for ϕ_{31}. Since we have obtained these results using the sliding mean calculations, it is difficult to determine the exact significance of these results specially at longer wavelengths, where the number of stars is smaller in the vicinity of $\log(P) = 1.0$. Since we applied the same procedure at all bands, there is a differential effect in these parameters that seems to be real. Also, this confirms the work of Beaulieu (1998), who has determined the centre of the HP for our Galaxy, LMC and SMC Cepheids using Fourier parameters. Beaulieu (1998) found a shift in the HP centre towards the longer periods for the Galaxy having lower mean metallicity, following the work of Andreasen & Petersen (1987) and Andreasen (1988). However, we emphasize that more data will be needed to determine the central period more accurately, particularly at longer wavelengths.

7 CONCLUSIONS

In the present study, we discussed the Fourier decomposition of Galactic and LMC Cepheid light curves in multiple bands. We compiled and made use of the largest data sets available in each band. We analysed the variation of Fourier parameters in detail to observe some interesting patterns. We found an increase in phase parameters with increasing wavelength for both Galactic and LMC variables. We also observed a decrease in amplitude parameters with increasing wavelength. An interesting pattern in amplitude parameters was observed, which suggests that for *VIJ* band, the amplitude parameters increases sharply as compared to longer wavelengths for periods greater than around 20 d. Quantitatively, this was summarized by determining the difference of mean Fourier parameters in multiple bands. We also observed a decrease in skewness and acuteness parameters as function of wavelength at a fixed period

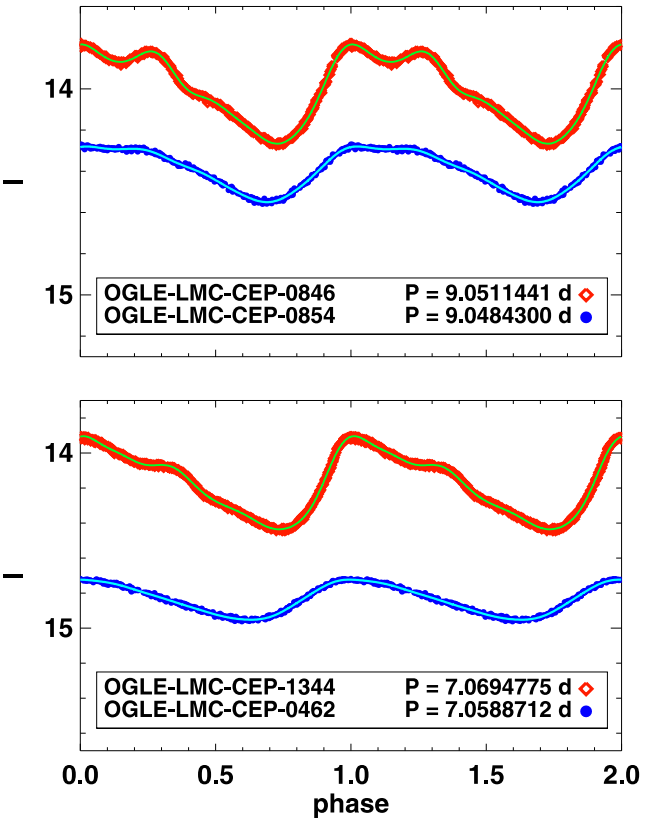

Figure 19. Examples of *I*-band light curves of LMC Cepheids, which have periods in the vicinity of clump in R_{31} parameters in Fig. 4. Light curves in red/blue colour are from in/outside of the clump, respectively.

suggesting Cepheid light curves to be more symmetric at longer wavelengths.

The central period of the HP displays a clear variation with increasing wavelength, suggesting an increase in central period for Fourier amplitude parameters and a decrease for phase parameters. At optical bands, the mean central period of the HP occurs at $\log(P) \sim 1.03$ for the Galaxy and at $\log(P) \sim 1.04$ for the LMC, which are consistent with the previous studies (Welch et al. 1997; Bono et al. 2000). We also found small differences in the central period of the HP for different Fourier parameters between the Galaxy and LMC. These differences are mainly in the R_{21} beyond K_s and in ϕ_{21} beyond *J*. These differences are such that Galactic data have the central period at shorter values. At optical bands, this difference is more accurate and confirms previous work by Beaulieu (1998) but we cannot determine the exact significance at infrared bands due to larger scatter in amplitude and phase parameters.

We also observed a flatter variation in R_{31} amplitude parameter as compared to other Fourier parameters in the vicinity of 10 d. This shallower minimum is more pronounced in the mean Fourier parameters shown in Figs 11 and 12. Further, we observed a clump in the R_{31} in the vicinity of $0.7 < \log(P) < 1.0$ for *VI* bands (see Fig. 4), which is a possible cause of flatter minimum in Fig. 12. However, this clump is not visible for Galactic Cepheids because of the smaller number of stars as compared to OGLE LMC data. We investigated the light curves of stars in/outside the clump but with similar periods. Examples are shown in Fig. 19. A slight bump after the maximum light (minimum magnitude) is observed in the light curves for the stars that are in the clump noted in the R_{31} versus $\log(P)$ plot (Fig. 4). This feature will be extensively studied in future work and may provide a direct link between light-curve structure and Fourier parameters.

The variation of Fourier parameters with wavelength can shed light on pulsation physics that are wavelength dependent. Further, these results can serve as a benchmark to constrain theoretical stellar pulsation models that now routinely incorporate model stellar atmospheres and produce light curves at various wavelengths.

While a physical interpretation of Fourier parameters is still an open question, the method does provide a quantitative description of the structure of Cepheid and RR Lyrae light curves. In order to have more confidence in these models, it will be important to compare these model and observed light curves, quantitatively with Fourier parameters as a function of metallicity, wavelength and period.

ACKNOWLEDGEMENTS

AB is thankful to the Council of Scientific and Industrial Research, New Delhi, for a Junior Research Fellowship (JRF) and to Sukanta Deb for helpful discussions. This work is supported by the grant provided by Indo-U.S. Science and Technology Forum under the Joint Center for Analysis of Variable Star Data. CCN thanks the funding from Ministry of Science and Technology (Taiwan) under the contract NSC101-2112-M-008-017-MY3. LMM acknowledges support by the United States National Science Foundation through AST grant number 1211603 and by Texas A&M University through a faculty start-up fund and the Mitchell-Heep-Munnerlyn Endowed Career Enhancement Professorship in Physics or Astronomy. We also thank the anonymous referee for his/her useful suggestions that improved the quality of the paper. This research was supported by the Munich Institute for Astro- and Particle Physics (MIAPP) of the DFG cluster of excellence 'Origin and Structure of the Universe'. This work has made use of NASA's Astrophysics Data System, SIMBAD data base and the VizieR catalogue, McMaster Cepheid Photometry data base and the data products from the Two Micron All Sky Survey.

REFERENCES

Andreasen G. K., 1988, A&A, 196, 159
Andreasen G. K., Petersen J. O., 1987, A&A, 180, 129
Antonello E., Poretti E., 1986, A&A, 169, 149
Baart M. L., 1982, IMA J. Numer. Anal., 2, 241
Barnes T. G., III, Fernley J. A., Frueh M. L., Navas J. G., Moffett T. J., Skillen I., 1997, PASP, 109, 645
Beaulieu J. P., 1998, Mem. Soc. Astron. Ital., 69, 21
Berdnikov L. N., 1987, Perem. Zvezdy, 22, 530
Berdnikov L. N., 1992, Sov. Astron. Lett., 18, 130
Berdnikov L. N., 1995, in ASP Conf. Ser. Vol. 83, The Cepheid Data Base. Astron. Soc. Pac., San Francisco, p. 249
Berdnikov L. N., Turner D. G., 2001, Astron. Astrophys. Trans., 19, 689
Berdnikov L. N., Turner D. G., 2004a, Astron. Astrophys. Trans., 23, 395
Berdnikov L. N., Turner D. G., 2004b, Astron. Astrophys. Trans., 23, 599
Berdnikov L. N., Vozyakova O. V., 1995, Astron. Lett., 21, 308
Berdnikov L. N., Yakubov S. D., 1993, Perem. Zvezdy, 23, 47
Berdnikov L. N., Ignatova V. V., Pastukhova E. N., 1998, Astron. Astrophys. Trans., 15, 81
Bhardwaj A., Kanbur S. M., Singh H. P., Ngeow C.-C., 2014, MNRAS, 445, 2655
Bono G., Marconi M., Stellingwerf R. F., 2000, A&A, 360, 245
Deb S., Singh H. P., 2009, A&A, 507, 1729
Deb S., Singh H. P., 2010, MNRAS, 402, 691
Deb S., Singh H. P., 2014, MNRAS, 438, 2440
Fernie J. D., Evans N. R., Beattie B., Seager S., 1995, Inf. Bull. Var. Stars, 4148, 1

Jurcsik J., Kovacs G., 1996, A&A, 312, 111
Kovacs G., Shlosman I., Buchler J. R., 1986, ApJ, 307, 593
Laney C. D., Stobie R. S., 1992, A&A, 93, 93
Leavitt H. S., Pickering E. C., 1912, Harv. Coll. Obs. Circ., 173, 1
Macri L. M., Ngeow C.-C., Kanbur S. M., Mahzooni S., Smitka M. T., 2014, preprint (arXiv:1412.1511)
Madore B. F., Freedman W. L., 1991, PASP, 103, 933
Monson A. J., Pierce M. J., 2011, ApJ, 193, 12
Monson A. J., Freedman W. L., Madore B. F., Persson S. E., Scowcroft V., Seibert M., Rigby J. R., 2012, ApJ, 759, 146
Moskalik P., Buchler J. R., Marom A., 1992, ApJ, 385, 685
Nemec J. M. et al., 2011, MNRAS, 417, 1022
Ngeow C.-C., Kanbur S. M., Nikolaev S., Tanvir N. R., Hendry M. A., 2003, ApJ, 586, 959
Ngeow C.-C., Lucchini S., Kanbur S., Barrett B., Lin B., 2013, preprint (arXiv:1309.4297)
Persson S. E., Madore B. F., Krzemiński W., Freedman W. L., Roth M., Murphy D. C., 2004, AJ, 128, 2239
Poretti E., 1994, A&A, 285, 524
Scowcroft V., Freedman W. L., Madore B. F., Monson A. J., Persson S. E., Seibert M., Rigby J. R., Sturch L., 2011, ApJ, 743, 76
Simon N. R., 1977, ApJ, 217, 160
Simon N. R., 1985, ApJ, 299, 723
Simon N. R., 1986, ApJ, 311, 305
Simon N. R., 1988, in Stalio R., Willson L. A., eds, Astrophysics and Space Science Library, Vol. 148, Pulsation and Mass Loss in Stars. Kluwer, Dordrecht, p. 27
Simon N. R., Davis C. G., 1983, ApJ, 266, 787
Simon N. R., Kanbur S. M., 1995, ApJ, 451, 703
Simon N. R., Lee A. S., 1981, ApJ, 248, 291
Simon N. R., Moffett T. J., 1985, PASP, 97, 1078
Simon N. R., Schmidt E. G., 1976, ApJ, 205, 162
Simon N. R., Teays T. J., 1982, ApJ, 261, 586
Soszynski I. et al., 2008, Acta Astron., 58, 163
Stellingwerf R. F., Donohoe M., 1986, ApJ, 306, 183
Stellingwerf R. F., Donohoe M., 1987, ApJ, 314, 252
Stetson P. B., 1996, PASP, 108, 851
Ulaczyk K. et al., 2013, Acta Astron., 63, 159
Welch D. L., Wieland F., McAlary C. W., McGonegal R., Madore B. F., McLaren R. A., Neugebauer G., 1984, ApJS, 54, 547
Welch D. L. et al., 1997, in Ferlet R., Maillard J.-P., Raban B., eds, Variables Stars and the Astrophysical Returns of the Microlensing Surveys. Editions Frontieres, Gif-sur-Yvette, p. 205

SUPPORTING INFORMATION

Additional Supporting Information may be found in the online version of this article:

Table 2. Fourier parameters obtained using a sine series Fourier fit to the Galactic Cepheid light curves in multibands.
Table 3. Fourier parameters obtained using a sine series Fourier fit to the LMC Cepheid light curves in multibands (http://mnras.oxfordjournals.org/lookup/suppl/doi:10.1093/mnras/stu2678/-/DC1).

Please note: Oxford University Press are not responsible for the content or functionality of any supporting materials supplied by the authors. Any queries (other than missing material) should be directed to the corresponding author for the paper.

This paper has been typeset from a TEX/LATEX file prepared by the author.